WPJET1-CPR(17) 17446

F Koechl et al.

W transport and accumulation control during the H-L transition of JET H-mode discharges and implications for ITER

Preprint of Paper to be submitted for publication in Proceeding of 44th European Physical Society Conference on Plasma Physics (EPS)

This work has been carried out within the framework of the EUROfusion Consortium and has received funding from the Euratom research and training programme 2014-2018 under grant agreement No 633053. The views and opinions expressed herein do not necessarily reflect those of the European Commission.

W transport and accumulation control in the termination phase of JET H-mode discharges and implications for ITER

F. Köchl[1,2], A. Loarte[3], E. de la Luna[4], V. Parail[1], G. Corrigan[1], D. Harting[1], I. Nunes[5], C. Reux[6], F. G. Rimini[1], A. Polevoi[3], M. Romanelli[1] and JET Contributors[*]

EUROfusion Consortium, JET, Culham Science Centre, Abingdon, OX14 3DB, UK
[1]Culham Centre for Fusion Energy, Culham Science Centre, Abingdon, OX14 3DB, UK
[2]Fusion@ÖAW, Atominstitut, TU Wien, Stadionallee 2, 1020 Vienna, Austria
[3]ITER Organization, Route de Vinon-sur-Verdon, CS 90 046, 13067 St Paul Lez Durance Cedex, France.
[4]Laboratorio Nacional de Fusión, CIEMAT, 28040 Madrid, Spain.
[5]IST, Instituto de Plasmas e Fusão Nuclear, Av Rovisco Pais, 1049-001, Lisboa, Portugal.
[6]CEA, IRFM, F-13108 Saint Paul-lez-Durance, France.

E-mail: Florian.Koechl@ukaea.uk

Abstract. Tokamak operation with W PFCs is associated with specific challenges for impurity control, which may be particularly demanding in the transition from stationary H-mode to L-mode. To address W control issues in this phase, dedicated experiments have been performed at JET including the variation of the decrease of the power and current, gas fuelling and central Ion Cyclotron Heating (ICRH), and applying active ELM control by vertical kicks. The experimental results obtained demonstrate the key role of maintaining ELM control to control the W concentration in the exit phase of H-modes with slow (ITER-like) ramp-down of the Neutral Beam Injection (NBI) power in JET.

For these experiments, integrated fully predictive core+edge+SOL transport modelling studies applying discrete models for the description of transients such as sawteeth and ELMs have been performed for the first time with the JINTRAC suite of codes for the entire transition from stationary H-mode until the time when the plasma would return to L-mode focusing on the W transport behaviour. Simulations have shown that the existing models can appropriately reproduce the plasma profile evolution in the core, edge and SOL as well as W accumulation trends in the termination phase of JET H-mode discharges as function of the applied ICRH and ELM control schemes, substantiating the ambivalent effect of ELMs on W sputtering on one side and on edge transport affecting core W accumulation on the other side. The sensitivity with respect to NB particle and momentum sources has also been analysed and their impact on neoclassical W transport has been found to be crucial to reproduce the observed W accumulation characteristics in JET discharges.

In this paper the results of the JET experiments, the comparison with JINTRAC modelling and the adequacy of the models to reproduce the experimental results are described and conclusions are drawn regarding the applicability of these models for the extrapolation of the applied W accumulation control techniques to ITER.

1. Introduction

Operation of tokamaks with tungsten (W) plasma facing components (PFCs) in the H-mode confinement regime presents specific challenges regarding the control of the impurity concentration in the main plasma. Lack of impurity control can lead to the loss of the H-mode, the radiative collapse of plasmas by W accumulation and increased disruptivity (cf. [de la Luna 2017]), which is detrimental to ITER operation. Control of W in H-mode plasmas requires, as a first step, the control of W production and of its transport into the core plasma through the SOL and edge transport barrier. In addition, even when the concentration of W at the pedestal is kept at low levels, unfavourable core W transport can lead to its uncontrolled accumulation and to loss of the H-mode due to increased radiation. Strategies have been developed in present experiments to avoid W accumulation in stationary phases of H-mode discharges by controlled ELM triggering to control the edge W density and central RF heating to prevent core accumulation. Such schemes are also expected to be effective in ITER, where

[*] See Appendix of F. Romanelli, et al., Proceedings of 25th IAEA Fusion Energy Conference 2014, Saint Petersburg, Russia

strong core W accumulation is not expected to occur due to the low particle source provided by the 1 MeV negative-NBI injection, which is in agreement with H-mode experiments with low core source [Loarte PoP 2015]. On the other hand, the control of W transport can be more challenging during the confinement transient phases between L-mode and H-mode and in particular in the transition from stationary H-mode to L-mode. During this phase the pedestal plasma density and temperature decrease as the input power is decreased and this can lead to reduced ELM frequencies and extended intermittent ELM-free phases causing uncontrolled increase of the edge W density and peaking of the core density profile, which is favourable for W accumulation. To avoid this, a frequently followed approach in present experiments is to cause a fast H-L transition and in this way increase the W outflux from the core preventing its accumulation. This approach is, however, not applicable to ITER high Q regimes both due to the impossibility to suddenly stop alpha heating and because the associated change in plasma energy would lead to direct contact of the plasma with the inner wall [Loarte NF 2014]. In addition, a slow decrease of the plasma energy in the H-mode termination phase is required to avoid excessive transient heat fluxes that may reduce the life-time of the PFCs. A slow transition to L-mode in ITER can, however, be prone to W accumulation [Loarte EPS 2015].

In order to address W control issues in the H-mode termination phase, a series of dedicated experiments have been performed at JET and modelled with the JINTRAC suite of codes [Romanelli PRF 2014]. In these experiments several H-mode termination scenarios with constant plasma current have been explored including the variation of the decrease of the power ramp rate, gas fuelling level and central ICRH heating with and without active ELM control. The required ELM frequency to avoid W accumulation can be achieved at JET through adjustment of the gas fuelling level (unlikely to be effective in ITER) or by active ELM control with pellets or kicks (fast vertical plasma motion at an adjustable frequency) [de la Luna NF 2016] at levels of gas fuelling for which W accumulation occurs when pellets / kicks are not applied. The latter scenario might provide an integrated solution regarding the control of W concentration and plasma energy evolution in the termination of H-modes that could be readily extrapolated to the corresponding phase of 15 MA Q = 10 plasmas in ITER.

The influence of certain aspects that were found to have a significant impact on the core W accumulation behaviour in the H-mode termination phase in the experiment and in previous modelling studies such as ELM control, NBI momentum and particle sources and ICRH have been analysed by means of integrated modelling attempts with JINTRAC. ELM control in particular has been identified to be crucial for the mitigation or prevention of core W accumulation in the H-mode termination phase in JET discharges in the modelling. There is ample experimental evidence of the beneficial impact of increasing the ELM frequency to avoid the development of enhanced W contamination of the core region, e.g. by means of gas injection [Neu PoP 2013] or a variation in plasma geometry and divertor pumping efficiency [Parail JNM 2015]. ELMs can in principle be detrimental for the prevention of core W accumulation, as they are responsible for a significant increase in W sputtering, and they can enhance the transport of W located in the edge region towards the core of this increased W influx. However, they can also have a positive effect for the maintenance of a low level of W density in the edge region due to depletion of the total edge+core W content caused by the particle expulsion and the subsequent modification of the pedestal density and temperature profiles that determine the neoclassical W screening efficiency in the pedestal. The balance of the possible effects of ELMs on W accumulation is, therefore, not trivial and this paper focuses on providing an assessment of such effects by integrated modelling of JET discharges in stationary H-mode conditions and in the H-mode exit phase.

This paper is structured as follows: The characteristics of the main JET experiments that have been analysed in this study are briefly described together with the integrated model assumptions and simulation conditions that have been applied in the JINTRAC calculations

in Section 2. Attempts for the validation of the integrated core+edge+SOL transport model applied in JINTRAC with discrete (i.e. non-time-averaged) treatment of ELMs and sawteeth for the stationary H-mode phase in JET discharges with vs. without ELM control are presented in Section 3. Integrated core+edge+SOL JINTRAC calculations with discrete ELMs and sawteeth for the analysis of the ITER-like H-mode termination phase in JET without ELM control leading to strong core W accumulation are described in Section 4. In Section 5, W core transport evolution in the H-mode termination phase and dependencies on heating schemes, sources and transport assumptions are assessed by means of JINTRAC simulations for the core+edge region with a simplified ELM transport model, benchmarked with the results achieved in the core+edge+SOL calculations with discrete ELMs. Section 7 describes simulations of the H-mode termination of ITER Q = 10 baseline scenario plasmas with the models which have been validated against the JET experiments and analyses the conditions in which W accumulation occurs in this phase and demonstrates operational strategies to avoid it; in addition, the similarities and differences between the JET and ITER plasmas regarding the W production and transport in this phase are discussed. Finally, a summary of the conclusions of the studies presented in this paper is provided in Section 7.

2. Experiments and modelling tools

2.1 JET H-mode termination experiments with vs. without ELM control

In a series of dedicated JET experiments, W transport and control conditions have been studied for an ITER-like H-mode termination where the power is ramped down gradually within a few seconds [de la Luna 2017]. Two discharges #90224 and #90223 of this series have been selected for detailed modelling analysis. The time evolution of plasma conditions in the H-mode termination phase for these shots is illustrated in Fig. 1. While ELMs are controlled by the application of vertical kicks at a frequency of 43 Hz until the end of the H-mode phase in #90224, ELM control has been deactivated in the late stationary H-mode and the H-mode termination phases for t > 11 s in #90223 with ELMs occurring at a much lower natural frequency of < ~24 Hz. The average energy loss per ELM was estimated to be close to ΔW_{ELM} ~ 90 kJ for #90224 in stationary H-mode, while it increases to ΔW_{ELM} ~ 140 kJ in #90223 at t > 11 s as expected for reduced f_{ELM}.

In both shots, core radiation remains relatively constant at a level of a few MW during the main heating phase up to t=11 s, where the ELM frequency is controlled by kicks. While the core radiation can be kept constant in #90224 with ELM control and a safe H-mode termination can be realised, $P_{rad,core}$ increases in #90223 in the late stationary H-mode phase without ELM control and reduced f_{ELM} at 11 s < t < 12 s and then rises sharply to peak values of ~ 10 MW in the H-mode termination phase when the power is ramped down and ELMs appear at an even lower frequency. This rise in core radiation seems to be caused by an increased flow of W to the very core of the plasma. It leads to a faster reduction in core energy content and a faster drop in heat flow at the separatrix, P_{sep}, that approaches the L-H transition threshold (P_{L-H}) triggering an intermittent L-H dithering phase at ~12.5 s < 13 s followed by a back transition to L-mode.

Modelling results for the stationary H-mode phase with controlled vs. natural ELMs (11 s < t < 12 s) in #90224 vs. #90223 and for the H-mode termination phase in #90223 (t > 12 s) are presented in Sections 3 and 4 respectively. JET H-mode termination experiments with an extended (ITER-like) vs. short power ramp phase have also been analysed. They are described together with modelling results in Subsection 5.5.

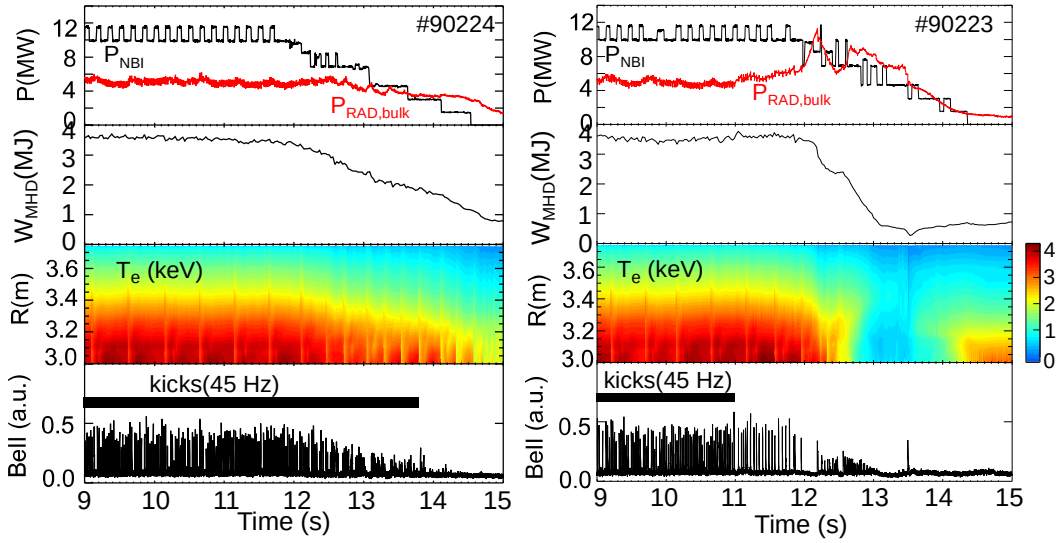

Figure 1. H-mode termination phase in JET discharges #90224 (left) and #90223 (right). From top to bottom: NB power (black) and core radiation (red), core energy content from equilibrium reconstruction estimates, electron temperature contour plot from ECE measurement, BeII signal (black) and indication of H-mode phase with ELM control by vertical kick application (grey). ELMs are controlled by kick application until the end of the H-mode phase in #90224 while ELM control has been deactivated in the late stationary H-mode and the H-mode termination phases for t > 11 s in #90223.

2.2 Simulation conditions

For the analysis of the H-mode termination experiments, fully predictive transport simulations have been carried out with JINTRAC in Coconut mode, i.e. for the core, edge and SOL region considering the interaction with PFCs by combination of the core transport code JETTO+SANCO with the SOL transport code EDGE2D+EIRENE. For the description of transport in the core and edge, transport equations are solved for q, p_e, p_i, n_D, n_{Be}, n_W, v_{tor}. Neoclassical transport is calculated by NCLASS [Houlberg PoP 1997] for main ions and all impurity stages except for W transport, which is described by application of a bundling scheme with six super-stages in SANCO [Summers AIP 2007], including the dominant correction terms for the consideration of poloidal asymmetry for high Z impurities at high core rotation from [Romanelli PPCF 1998], while anomalous transport is described by the gyro-Landau fluid model GLF23 [Waltz PoP 1997] in H-mode (considering impurity specific anomalous transport predictions) and by the standard Bohm/gyroBohm model [Erba JET-R 1996] (including an inwards pinch term proportional to $0.5 \cdot D_{i,BgB}$) in L-mode. Impurity reaction cross-sections are evaluated by ADAS, with W cooling rates being calculated from ADAS datasets based on [Pütterich PPCF 2008]. Transport in the ETB is modelled by applying a reduction of anomalous transport diffusivities in the ETB, $D_{ETB,anom}$, $\chi_{e,i,ETB,anom}$ (towards neoclassical values), which depends exponentially on the margin of the edge power flow (P_{net}) over the LH transition (P_{L-H}) power as $\exp(-(P_{net}-P_{L-H})/(\lambda \cdot P_{L-H}))$, where $P_{net} := P_{in} - dW_{th}/dt - P_{rad}$, as described in [Loarte NF 2014]. The values of the parameter λ for $D_{ETB,anom}$ and $\chi_{e,i,ETB,anom}$ have been inferred from JET L-H transition studies with carbon-based plasma facing components [Koechl NF 2017] for which $\lambda_D = 0.08$, $\lambda_{\chi_{e,i}} = 0.20$. In the present studies, the L-H transition power threshold P_{L-H} is evaluated according to the scaling in [Martin JoP 2008] scaled by 0.7, as found to be appropriate to describe the L-H power threshold in JET ILW discharges [Maggi NF 2014]. With these assumptions, anomalous particle transport is more efficiently suppressed in the barrier zone than anomalous heat transport when H-mode confinement is accessed. The latter can remain significant also in a fully developed stationary H-mode regime with values of $\chi_{e,i,ETB,anom}$ far above those expected from neoclassical transport. Resistivity and bootstrap current density are calculated by

NCLASS. Momentum transport coefficients are assumed to be equal to the ion heat transport coefficients (Prandtl number equal one) considering both anomalous and neoclassical contributions.

Sawteeth are treated as instantaneous events applying the Porcelli sawtooth reconnection model [Porcelli PPCF 1996]. ELM events are modelled discretely by transient application of additional heat and particle diffusivities D_{ELM}, $\chi_{e,i,ELM}$ in the edge region for the duration of the ELM. A Gaussian shape distribution is assumed for D_{ELM}, $\chi_{e,i,ELM}$ with peak values of 10 m^2/s being achieved at a location $\rho_{tor,norm} \sim 0.98$ and a full width at half maximum of ~0.22 in terms of $\rho_{tor,norm}$ which determines the ELM affected area. The additional ELM diffusivities are linearly ramped to the maximum within ~300 μs, then maintained constant until a prescribed loss in energy per ELM ΔW_{ELM} that is determined from measurements is achieved and finally ramped down linearly within ~100 μs. The experimental time-averaged ELM frequency is prescribed in the simulation, i.e. no MHD stability analysis is carried out to determine the ELM trigger times for simplicity.

Auxiliary heating by neutral beams and ICRH heating are modelled with the PENCIL [Challis NF 1989] and PION [Eriksson NF 1993] codes respectively, while ECRH (in ITER simulations) is modelled with a scaling approximation based on GRAY calculations [Farina FSciTec 2007].

Plasma fuelling is realised by high energy neutrals from the neutral beams, neutral atoms originated from gas puffing prescribing the experimental gas puff rates and (approximately) the experimental gas puff locations, by plasma recycling (applying a wall recycling coefficient of 1.0 for D) and, in case of ITER simulations, by pellets with a continuous pellet source with a peak in particle deposition at $\rho_{norm} \sim 0.85$ (cf. [Pégourié PPCF 2009]).

The magnetic equilibrium is updated every ~100 ms with the 2D equilibrium solver ESCO (considering the pressure contribution from fast particles).

Standard JET wall and pump structures and assumptions are applied [Romanelli PFR 2014, Groth JNM 2015]. The standard Braginski model is used for the parallel heat and particle transport in the SOL [Braginski RevPP 1965]. Perpendicular transport is described by a model with radially dependent coefficients as described in [Wiesen PPCF 2011]. In the near-SOL, it is assumed to be equal to its 1-D counterpart at the separatrix. Further away from the separatrix (at $R\text{-}R_{sep} > \sim 0$ / 0.5 cm in the outer midplane in L-mode / H-mode resp.) the heat and particle diffusivities are assumed to gradually approach a constant level for reasons of continuity, with fixed prescribed far-SOL values of $\chi_e = \chi_i = 1.0\ m^2/s$, $D_{D/T} = D_{imp} = 0.3\ m^2/s$. Cross-field drifts in the SOL are not included in the simulations.

The maximum time step used for the integration of the transport equations in EDGE2D is set to 5 μs between ELMs and reduced to 0.5 μs during and for a few ms after ELM events until quasi-stationary conditions in the SOL are re-established. To reduce the required computation time for these CPU-intensive simulations, a partial coupling scheme is applied in the later (quasi-stationary) inter-ELM phases with a maximum ratio of 15 ms : 1 ms between phases when JETTO+SANCO and EDGE2D+EIRENE are coupled and boundary conditions are exchanged at each time step and phases without coupling and JETTO+SANCO being evolved at fixed boundary conditions. A partial coupling correction scheme is applied in which correction particle source terms are introduced to minimise the error in the time-averaged evolution of SOL particle content time derivatives with respect to an exact calculation without partial coupling. The partial coupling ratio is automatically reduced by the correction scheme if the correction particle source terms become sizeable to further reduce the error caused by the application of partial coupling. Partial coupling is automatically switched off at ELM trigger times as a higher precision in the calculation is required during and after the ELM when strong transients occur in the edge and SOL plasma evolution. For the

description of neutral dynamics, 12000 Monte Carlo particles have been used in EIRENE at each EIRENE iteration which is carried out every ~1-20 EDGE2D time steps. Regarding other edge modelling assumptions, the standard EDGE2D+EIRENE plasma-wall interaction models are used. The same set of impurities is considered in EDGE2D+EIRENE as with JETTO+SANCO. The effect of W self-sputtering has been considered. Prompt W re-deposition is roughly approximated by application of a scaling factor of $\xi_W = 0.2$ to the calculated W sputtering yield.

In the JINTRAC simulations for the core+edge region only presented in Sections 5 and 6, ELM transport is modelled in a time-averaged way with the continuous ELM model [Parail NF 2009]. The core influx of Be and W is feedback controlled against the experimental Z_{eff} and P_{rad} respectively. Other boundary conditions that need to be prescribed at the separatrix in these simulations are roughly matched with modelling results from core+edge+SOL transport calculations of similar edge plasma conditions presented in Sections 3 and 4.

3. Modelling benchmark in stationary H-mode conditions

JINTRAC core+edge+SOL simulations have been carried out for the late stationary H-mode phase t = 11 – 12 s in discharges #90223 and #90224. While both discharges are run with identical conditions for t < 11 s, the plasma evolution deviates in this phase, as ELM control by vertical kick application is switched off at t = 11 s in #90223 while it is maintained in #90224. For that reason, f_{ELM} immediately drops to the natural ELM frequency of ~23.5 Hz for t > 11 s in #90223, while a much higher f_{ELM} ~ 43 Hz is maintained in #90224. Likewise, the energy loss per ELM is immediately increased to ~140 kJ in #90223 while is kept at a low level of ~90 kJ in #90224. In analogy to the experiments, simulation conditions are identical for the JINTRAC simulations for #90223 and #90224 with the only exception of f_{ELM} and ΔW_{ELM} which are prescribed to the corresponding level observed in the experiment. In addition, initial conditions at t ~ 11 s are exactly the same for both simulations. Observed differences in simulation results are therefore not related to initial conditions. Prescribed profiles at the beginning of the simulations should roughly correspond to measurements for the stationary H-mode phase at t < 11 s when plasma characteristics are still the same and ELMs are controlled by kick application in both discharges #90223 and #90224, however, plasma rotation has been assumed to be close to zero at the beginning of the simulations due to the lack of reliable rotation measurements. Changes in plasma conditions in the early phase of the simulation (t < ~11.5 s) are therefore not only related to small differences between the initially prescribed measured and modelled density and pressure profiles for stationary H-mode but mainly to the build-up of core rotation in the simulation and the associated variation in core transport conditions.

A comparison of selected time traces for the simulations of #90223 and #90224 is shown in Figs. 2-3, demonstrating that the simulations reproduce well the experimental observations. As can be seen in Fig. 2, the change in ELM characteristics causes noticeable differences in pedestal conditions. At lower f_{ELM} (#90223), the temperature on top of the pedestal tends to decrease while the density on top of the pedestal rises with respect to the case where a high ELM frequency is maintained (#90224). This effect is associated with the well-known phenomenon of density depletion occurring at higher f_{ELM}. It is due to an increase in the time averaged ratio between particle vs. heat conductivities in the pedestal $\langle D_{ETB}/\chi_{ETB}\rangle_t$ in case of more frequent ELMs, as D_{ELM}/χ_{ELM} is significantly higher with respect to $D_{inter\text{-}ELM}/\chi_{inter\text{-}ELM}$. In the inter-ELM phase, D_{ETB} almost drops down to the neoclassical level while $\chi_{e,i,ETB}$ stays well above $\chi_{e,i,ETB,neocl.}$. In the simulation, this difference is achieved by application of different coefficients λ_D, $\lambda\chi_{e,i}$ in the L-H transition model fulfilling condition $\lambda_D < \lambda\chi_{e,i}$. It is important to note that the experimental quasi-stationary H-mode pedestal conditions can only

be matched appropriately with this assumption. This is a general finding for JET H-mode plasmas, as it was also found to be required for the description of the modelling of the plasma behaviour in the transition from L-mode to stationary H-mode in JET C-wall experiments [Koechl NF 2017].

Once quasi-stationary conditions are reached in the simulation, ratios $|\nabla n_{e,ped,\#90223}| / |\nabla n_{e,ped,\#90224}| \sim 1.50$ and $|\nabla T_{e,ped,\#90223}| / |\nabla T_{e,ped,\#90224}| \sim 0.85$ are achieved for the inter-ELM phase. These differences in pedestal properties have a significant impact on impurity (W, in this case) neoclassical convection in the ETB. Qualitatively, the neoclassical W convective velocity is proportional to the difference in the relative gradients of main ion density and temperature, $v_{neocl.} \propto \nabla n_i/n_i - 1/2 \cdot \nabla T_i/T_i$ [Hirshman NF 1981]. The transport of W through the barrier region towards the core can thus be indirectly influenced by the ELM frequency due to a modification of neoclassical W convection triggered by a change in pedestal conditions. An increased inflow to the core or a reduced outflow of W from the core in the inter-ELM phase can be expected at reduced f_{ELM} due to the associated increase in $|\nabla n_{i,ped}|$ and reduction in $|\nabla T_{i,ped}|$.

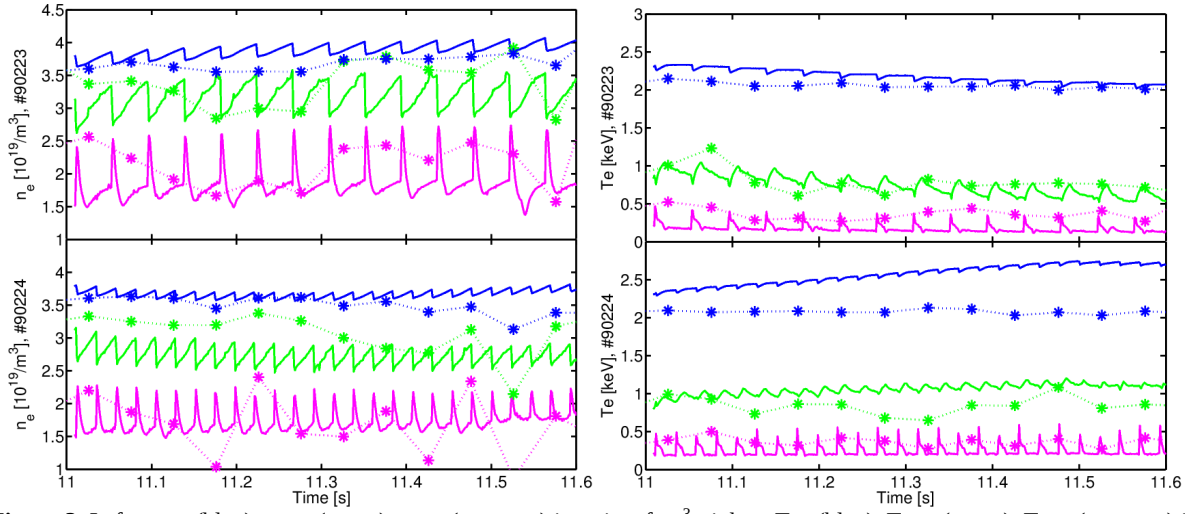

Figure 2. Left: $<n_e>$ (blue), $n_{e,ped}$ (green), $n_{e,sep}$ (magenta) in units of m^{-3}, right: $<T_e>$ (blue), $T_{e,ped}$ (green), $T_{e,sep}$ (magenta) in units of eV, for JINTRAC simulations of steady-state H-mode conditions at 11 s < t < 11.7 s (solid, evolving from imposed initial conditions at t ~ 11 s) vs. measurement data from High resolution Thomson scattering (HRTS, stars) at low natural ELM frequency $f_{ELM} \sim 23.5$ Hz with $\Delta W_{ELM} \sim 140$ kJ in #90223 (top) and high controlled ELM frequency $f_{ELM} = 43$ Hz with $\Delta W_{ELM} \sim 90$ kJ in #90224 (bottom).

Indeed, the W accumulation efficiency appears to be increased at lower ELM frequency. Both the core W concentration $c_W = <n_W>/<n_e>$ and the core radiation are significantly enhanced in the simulation with low f_{ELM} as shown in Fig. 3. This is, in part, the consequence of an increased inflow of W between ELMs at low f_{ELM} that is more pronounced due to the fact that the inter-ELM phase with fully developed pedestal lasts longer and the time available for the increase of the inwards neoclassical W convection to the core between ELMs is increased at low ELM frequency. The hypothesis of an increased inter-ELM W inflow is confirmed by the evolution of c_W which increases between ELMs in the simulation of #90223 at natural ELM frequency until a higher core W concentration level is reached, and the enhanced neoclassical inwards convection of W becomes compensated by an increased outwards-directed diffusive transport at higher core W density gradients.

However, the increase in neoclassical inter-ELM W convection is not the only reason for the observed rise in c_W at low f_{ELM}. Other mechanisms must be at play as well, as c_W is not only continuously increased between ELMs, but the W concentration also rises in an almost stepwise form immediately after an ELM event in a phase when the pedestal has not yet fully

been re-established and neoclassical W convection might actually be temporarily directed outwards due to a faster formation of the pedestal in temperature as compared to the pedestal in density [Parail JNM 2015].

According to modelling results, this sudden ELM-induced increase in c_W is caused by enhanced sputtering of W at the target plates due the increase in heat and particle fluxes during ELM events. The W that has been released is quickly transported through the SOL to the confined plasma region. The W density at the separatrix is increased above the pedestal W density level and an inward diffusion of W into the pedestal region takes place causing a rise in the core W concentration.

The increase in c_W due to inwards diffusion of sputtered W is in contrast to the direct effect of ELMs on W transport: as the diffusion in the ETB is strongly increased for the duration of the ELM in the simulation, W is transported from the confined region to the SOL while $n_{W,sep} < n_{W,core}$. Due to this effect, c_W drops down temporarily during ELM events before the sputtered W arrives at the core and c_W is sharply increased as seen in Fig. 3.

Apart from an outward diffusion of W towards the SOL as a consequence of enhanced diffusion caused by an ELM, D_{ELM} may also trigger an inwards diffusion of W from the edge to the core region in case that $n_{W,ETB} > n_{W,core}$. The latter condition is indeed fulfilled in the simulations. This effect is illustrated by a contour plot of the W density for both cases at low and high f_{ELM} in Fig. 4. Peaks in W density that appear in the pedestal zone in the inter-ELM phase are completely removed by ELM events. The W particles present in the ETB region are partly transported outwards towards the SOL leading to a reduction in c_W. At the same time, other W particles are transported from the ETB towards inner core regions. W then starts to accumulate in the very core where it is confined by an inwards directed neoclassical convective W velocity near the magnetic axis whose magnitude is increased in the presence of significant toroidal rotation due to rotation-induced poloidally asymmetric distributions of the W density causing an enhancement of neoclassical transport [Romanelli PPCF 1998] (cf. Fig. 4).

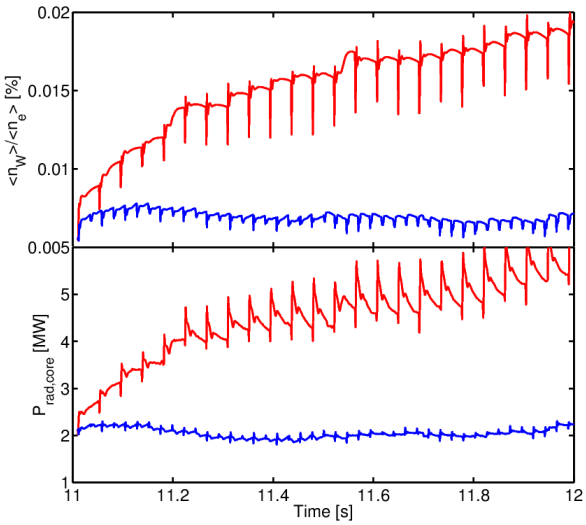

Figure 3. Top: W core concentration $\langle n_W \rangle / \langle n_e \rangle$, bottom: core radiation $P_{rad,core}$ (in W) for JINTRAC simulations of steady-state H-mode conditions at 11 s < t < 11.7 s (evolving from imposed initial conditions at t ~ 11 s) at low natural ELM frequency f_{ELM} ~ 23.5 Hz with ΔW_{ELM} ~ 140 kJ in #90223 (red colour) and high controlled ELM frequency f_{ELM} = 43 Hz with ΔW_{ELM} ~ 90 kJ in #90224 (blue colour).

It should be noted that ELMs are modelled to have a diffusive effect on particle transport in the simulations presented here. This assumption emulates the processes that are known to take place at the plasma edge during ELMs. These include reconnection of field lines and expulsion of plasma filaments and cause an effective flattening of the plasma profiles at the

edge (typically the plasma is affected up to r/a ~ 0.8 by ELMs [Loarte PPCF 2003]; this is approximately achieved in our modelling by application of enhanced edge diffusivities as described in Section 2. As discussed in detail later, there is initial experimental evidence that the inwards directed transport of W from the edge to the core region due to ELMs that is obtained in the simulations with this diffusion-based approach may be larger than in experiments.

The main direct effects of ELMs on W transport in the edge region are illustrated in Fig. 5 where a contour plot of the time evolution of the difference in n_W with respect to the W density at a selected time just before the occurrence of an ELM is shown. These effects can be summarised as follows:

1. Removal of W located in the edge region ($\rho_{norm,tor}$ ~ 0.94-0.98 in this simulation) causing a reduction of the overall core W content.
2. Partial inwards diffusion of W from the edge towards the core causing an increase in n_W with respect to the pre-ELM W density in the outer core region near the pedestal top location ($\rho_{norm,tor}$ ~ 0.87-0.93) a few milliseconds after the ELM crash that widens with time towards the core with the amplitude of the W density perturbation being reduced at the same time.
3. Appearance of W that has been sputtered at the target plates during the ELM at the separatrix with a delay of a few milliseconds causing an increase in $n_{W,sep}$ and an inwards diffusion of W from the SOL to the confined region and replenishment of the W particle content in the edge region.

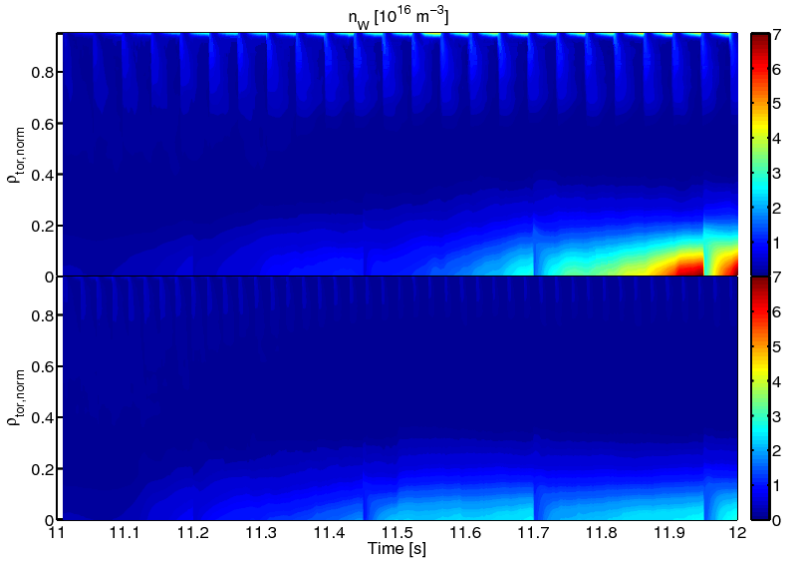

Figure 4. Contour plot of W density in core region 0.0 < ρ_{norm} < 0.95 <n_W>/<n_e> for JINTRAC simulation of steady-state H-mode conditions at 11 s < t < 12 s (evolving from imposed initial conditions at t ~ 11 s) at low natural ELM frequency f_{ELM} ~ 23.5 Hz with ΔW_{ELM} ~ 140 kJ in #90223 (top) and at high ELM frequency f_{ELM} ~ 43 Hz with ΔW_{ELM} ~ 90 kJ in #90224 (bottom).

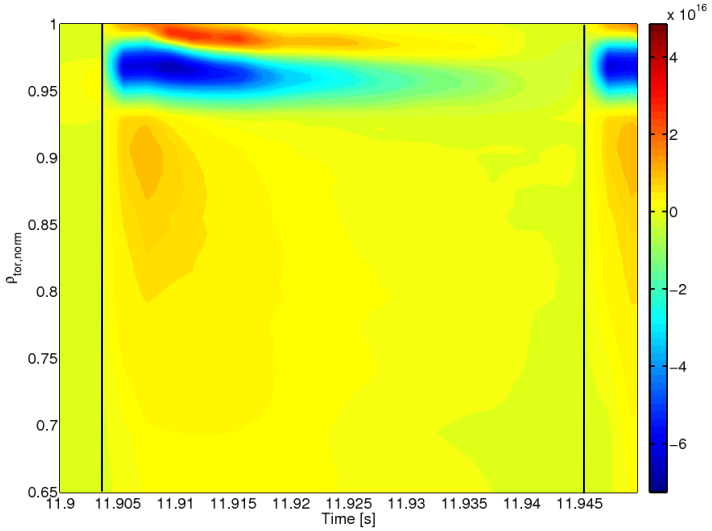

Figure 5. Contour plot of the time evolution of the difference in W density (in m^{-3}) in the outer core and ETB regions $0.65 < \rho_{norm} < 1.00$ with respect to the W density at the end of the inter-ELM phase evaluated at $t \sim 11.90$ s at 11.9 s < t < 11.95 s for JINTRAC simulation of steady-state H-mode conditions at low natural ELM frequency $f_{ELM} \sim 23.5$ Hz with $\Delta W_{ELM} \sim 140$ kJ in #90223. ELM trigger times are indicated by black vertical lines.

The rise in $n_{W,sep}$ after each ELM is also shown in Fig. 6 together with the evolution of the W density on axis for the simulation at low natural ELM frequency (#90223). $dn_{W,ax}/dt$ increases with time, i.e. the process of W accumulation in the very core of the plasma appears to be self-accelerating. This is a well-known effect that is regularly observed in the experiment and that is related to the change in core profiles: the temperature gradient near the magnetic axis is decreased as a consequence of enhanced W-induced radiation causing a further increase of the inwards directed neoclassical W convection due to reduced temperature screening. At the same time, density and rotation in the very core of the plasma are found to increase further, as the region where the inverse normalised temperature gradient length $L_T^{-1} = -\nabla T/(a_0 T)$ remains below the stiffness threshold widens leading to very low levels of anomalous transport in the plasma core. This leads to an increase of density and rotation in the core plasma and over a wider plasma region, which expands in time as the particle and momentum sources remain unchanged. The increase in density gradients and plasma rotation in the very core region cause the enhancement of the neoclassical inwards W convection due to a further reduction in temperature screening and a more pronounced rotation-induced neoclassical W transport enhancement and further accelerate the accumulation of W in the plasma centre. In the case with high f_{ELM} (#90224) a peak in W density appears as well in the very core of the plasma, however, it is small in amplitude and it does not increase in size, as the radiation associated to it is too small to noticeably affect the core temperature, momentum and density profiles. For that reason, the process of a self-accelerating W accumulation in the core is not triggered (cf. n_W contour plot for #90224 in Fig. 4).

While the neoclassical W convective velocity $v_{W,neocl.}$ is always inwards directed in the very core of the plasma, it may change sign both as a function of time and space in the plasma edge region. Fig. 6 includes a graph indicating the time evolution of $v_{W,neocl.}$ at the separatrix. While $v_{W,neocl.,sep.}$ appears to be inwards directed reaching very large negative values of ~ -70 m/s in the inter-ELM phase, the neoclassical W convection changes sign during and a few milliseconds after an ELM before the pedestal is re-established, causing a further temporary reduction in the core W concentration in addition the reduction in c_W that is due to the increase in edge diffusion due to the ELM. In addition, $v_{W,neocl}$ also changes sign as a function of the radial location within the barrier zone as illustrated in Fig. 7 for the inter-ELM phase. Within a few centimetres on the outer mid-plane, $v_{W,neocl}$ is predicted to increase by ~ 80 m/s

between the separatrix and the location of the top of the pedestal reaching positive peak values of ~ 20 m/s in the inner ETB region. As a consequence of such a sharp variation in W convection, a pronounced peak in W density is formed in the pedestal region as can be seen as well in Fig. 7. This peak can be maintained throughout the inter-ELM period with W being continuously transported towards the peak location from both sides due to the strong convection compensating diffusive losses in stationary conditions.

The presence of such a peak in W density within the pedestal can have a significant impact on details in the shape of kinetic profiles in that region. In particular, the temperature profiles can be affected, as the W peak would cause a strong localised peak in radiation and thus a heat sink that can lead to an increased reduction in temperature at the radiation peak location and reduced temperature gradients further outside. This temperature reduction can cause a change in the density profile shape in the pedestal and an increase of $|\nabla n|$ outwards from the pedestal temperature top by a corresponding increase of the neutral ionisation source in the pedestal itself. This source is low near the pedestal top but significant near the separatrix due to the lower temperatures, reducing the temperature difference between pedestal top and separatrix thus naturally increases ionization sources in the ETB itself. As a result, the density gradient is almost unchanged near the pedestal temperature top (ρ_{TOP}) but is strongly increased near ρ_{sep}. Indeed the temperature and density gradients within the barrier zone are not constant in the simulation and they vary in a way that is compatible with the presence of the peak in W density and a significant source of cold neutrals. This is not surprising as the simulations are supposed to be fully self-consistent, however, the same variation in density vs. temperature pedestal gradients is also observed in the experiment (cf. Fig. 8). This experimental evidence is thus consistent with the modelled W density enhancement within the ETB, at least in the discharges that have been analysed.

The opposite trends in the pedestal variations of $|\nabla T|$ vs. $|\nabla n|$ affect the neoclassical transport conditions in a way that a self-sustained process is established in the pedestal zone: Namely, it follows that temperature screening is effective in the inner ETB region but ineffective further outside near the separatrix. This difference entails the formation of a pronounced gradient in the neoclassical W convection velocity between the pedestal top and the separatrix, which in turn is responsible for the appearance of a peak in W in the ETB and the associated change in the pedestal temperature and density profile shape. The cold neutral ionisation source may be coupled to this cycle in the following way: The gradient in $|v_W|$ within the ETB is further increased due to the variation in $|\nabla n|$ associated to neutral ionisation, n_W within the ETB may further increase, the associated rise in radiation may cause a further reduction in P_{sep} which in turn could lead to an enhanced rate of cold neutrals reaching the confined region and increased neutral ionisation in the pedestal. Due to both causality chains (visualised in Fig. 9), the edge W peak appears to be robust and stable in the inter-ELM phase.

As a consequence of the difference in pedestal variations of $|\nabla T|$ vs. $|\nabla n|$ a visible shift appears in the effective location of the density pedestal vs. the temperature pedestal with the former being located further outwards with respect to the latter as illustrated in Fig. 8. Such a shift can be evaluated for instance as the difference between locations with maximum $|\nabla n|$ vs. maximum $|\nabla T|$. Interestingly, there are sparse indications that the effective shift between temperature and density pedestals might indeed be enhanced in certain JET experiments with the ITER-like wall with W coated targets in plasma conditions that are prone to develop strong core W accumulation. One may hypothesise that this enhanced shift could in such cases be associated to significant W accumulation in the barrier region. To confirm whether this is indeed the case, a detailed validation study may need to be carried out which is out of the scope of this paper.

Regarding W sputtering, it is important to note that the scaling factor ξ_W = 0.2 that is applied to the calculated W sputtering yield should only be considered as a very rudimentary approach for the consideration of prompt W re-deposition, even though the W sputtering source obtained with this assumption provides reasonable agreement in terms of W core accumulation behaviour and ELM-caused instant radiation (see below) between modelling and the experiments under consideration in both qualitative and quantitative terms. For an improved treatment of prompt W re-deposition, space and time dependent correction factors need to be applied to the W sputtering yield based on models as described in [Naujoks NF 1996, Chankin PPCF 2014]. Preliminary estimates suggest however that the net amount of W sputtered during ELMs on the basis of re-deposition factors derived from those models are lower than those required for the model to reproduce the (indirectly) observed W source in the experiment, under the assumption that the amount of W sputtered in the inter-ELM phase is relatively small compared to that during the ELMs, as suggested e.g. in [Kirschner EPS 2017] and can be neglected. There are of course many uncertainties (accuracy of W cooling rates, details in description of ELM dynamics such as ELM heat flux limiter and kinetic correction assumptions, perpendicular W transport dynamics in the SOL and boundary conditions such as for the W parallel velocity at the target plates) that may influence estimates of the required W source and the W re-deposition factor. In general, the assumptions in the simulations are conservative with respect to the W cooling rates (selected cooling rates from [Pütterich PPCF 2008] being in the upper range of available estimates). On the other hand the boundary condition for the W parallel velocity at the target plates (assuming that the latter is equal to the sound speed of W), does not consider the possibility of an increase of the W velocity to supersonic values towards the target due to collisions with main ions. These larger W velocities would lead to an increase of W production by self-sputtering but also to larger W losses to the divertor, as the timescale for W parallel transport in the SOL decreases, so that the net effect on the effectiveness of W produced at the divertor to reach the confined plasma can increase or decrease depending on the detailed balance of these effects in space and time during the ELM. An assessment of the balance of all these factors regarding core plasma contamination by W produced at the divertor requires detailed experimental and modelling investigations, which will be carried out but are outside the scope of this paper.

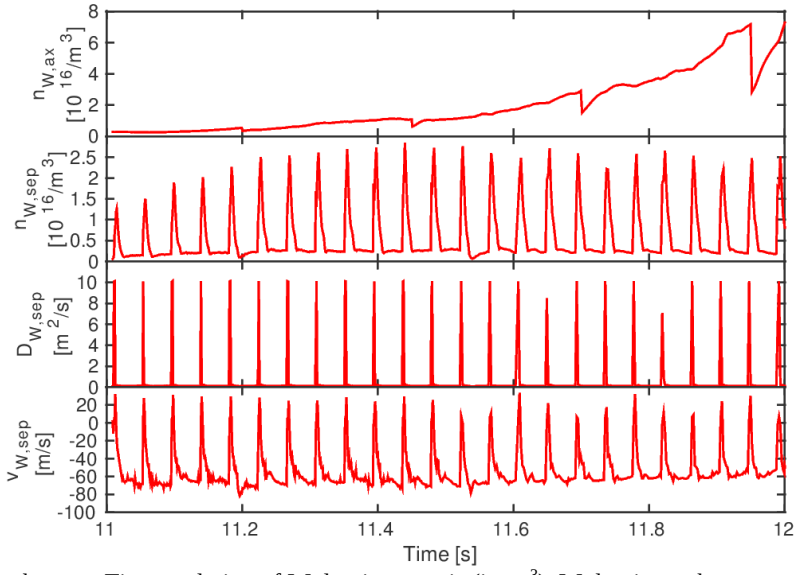

Figure 6. From top to bottom: Time evolution of W density on axis (in m^{-3}), W density at the separatrix (m^{-3}), W diffusion coefficient (m^2/s) and W convection velocity (m/s) at the separatrix, for the JINTRAC simulation of steady-state H-mode conditions at 11 s < t < 12 s at low natural ELM frequency f_{ELM} ~ 23.5 Hz with ΔW_{ELM} ~ 140 kJ in #90223.

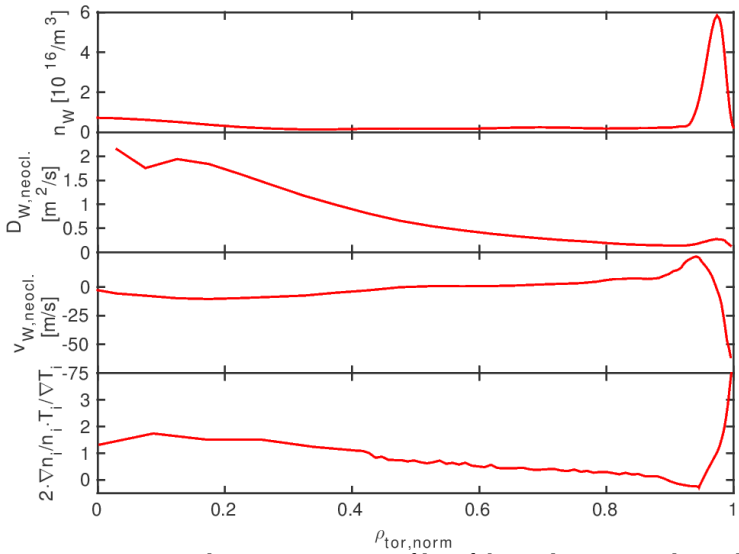

Figure 7. From top to bottom: Time-averaged inter-ELM core profiles of the W density, neoclassical W diffusion coefficient, neoclassical W convection velocity and 2x the ratio between ion temperature and density gradient lengths, for JINTRAC simulation of steady-state H-mode conditions at low natural ELM frequency f_{ELM} ~ 23.5 Hz with ΔW_{ELM} ~ 140 kJ in #90223 (evaluated at t ~ 11.3 s).

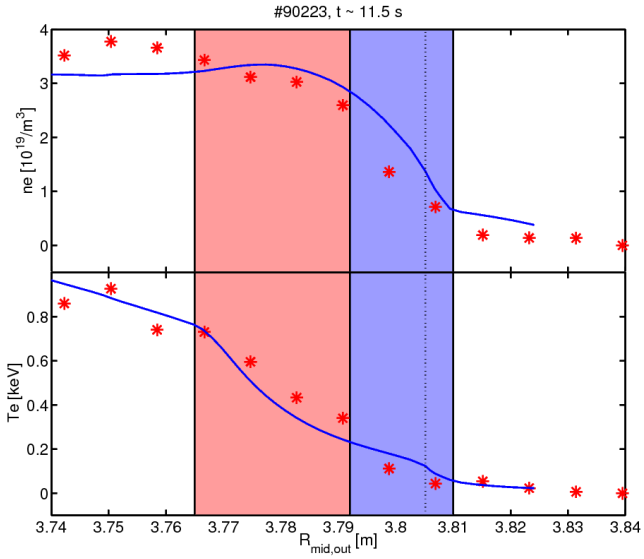

Figure 8. Comparison between measured (HRTS, red stars) and simulated (JINTRAC, blue colour) electron density (top) and electron temperature (bottom) profiles in the plasma edge region ($R_{mid,out}$ ~ 3.74-3.84 m) for #90223, t ~ 11.5 s. The position of the separatrix is indicated by a dashed line. The ETB region where |∇Te| reaches a maximum is highlighted in red colour, the region wih maximum |∇ne| is marked in blue colour.

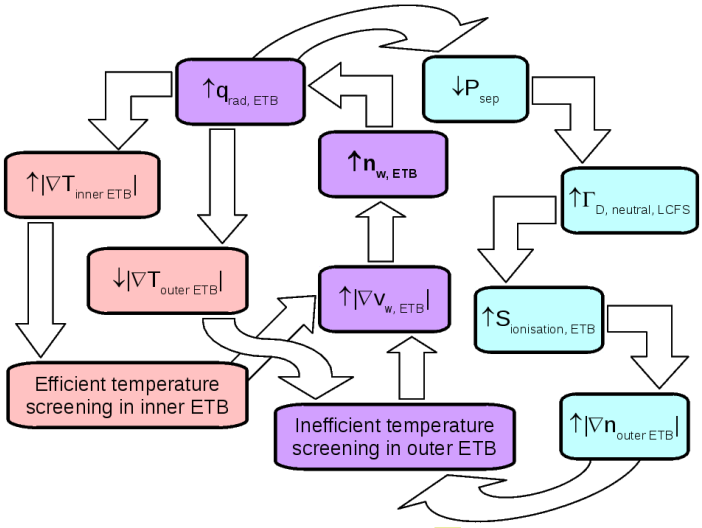

Figure 9. Visualisation of causality chains responsible for the appearance of a self-sustained peak in W density within the ETB in the inter-ELM phase in stationary H-mode in the JINTRAC simulations.

A comparison between available divertor measurement data and simulation results for the quasi-stationary H-mode phase is shown in Figs. 10-11. Peak values in divertor radiation during ELMs of the order of ~2 MW appear to be reasonably well reproduced in the simulations on the basis of the W radiation emitted during these events. This and the capability of the modelling to reproduce the W behaviour inside the separatrix in a quantitative way, justifies the appropriateness of the assumptions regarding the mechanisms for W production, re-deposition and transport discussed above as block (not each one individually). Likewise, the absolute value of the D_α signal is well matched for both the inner and outer divertor between ELMs. However, the predicted dynamic evolution of the D_α emission during ELM cycles is quite different between modelling and experiment, especially for the outer divertor. Although a reduction in D_α emission during the ELM event is known to be a signature for "negative" ELMs associated to a transition from detached inter-ELM to attached intra-ELM divertor conditions [Loarte NF 1998], in our modelling presented here this outer divertor D_α reduction is caused by a small relative increase in electron temperature whose effect on deuterium radiation is compensated by a significant reduction in the neutral density. The increase in temperature is not very pronounced, as T_e is already quite high in the late inter-ELM phase with maximum values of ~100 eV being reached near the strike-point location. The outer divertor is predicted to remain attached throughout the ELM cycle.

Overall, the agreement between measurements and simulations both for the confined region and the SOL appears to be sufficient to conclude that the integrated transport and source models that are implemented in JINTRAC feature all required physics mechanisms for a sufficiently accurate reproduction of the main trends observed in the experiment at least for the quasi-stationary ELMy H-mode phase. Based on this validation, the JINTRAC model is also applied to the prediction of the H-mode termination phase with the main results being presented in the next section.

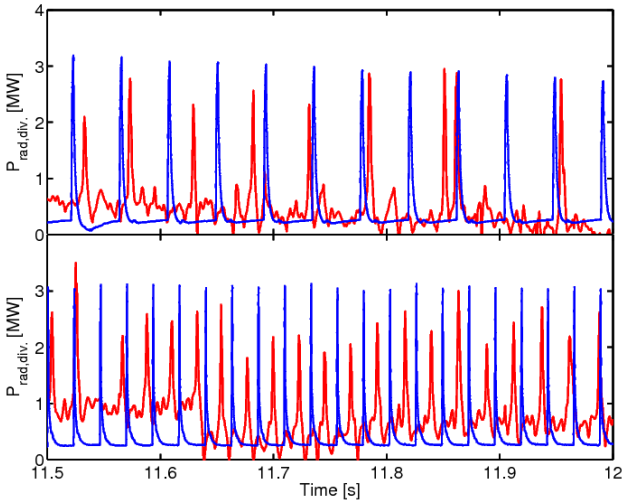

Figure 10. Time evolution of divertor radiation from bolometer measurements (red) vs. modelled time evolution of divertor radiation (including a minor contribution of SOL main chamber radiation) calculated with JINTRAC (blue) for steady-state H-mode conditions at 11 s < t < 12 s at low natural ELM frequency f_{ELM} ~ 23.5 Hz with ΔW_{ELM} ~ 140 kJ in #90223 and at high ELM frequency f_{ELM} ~ 43 Hz with ΔW_{ELM} ~ 90 kJ in #90224 (bottom).

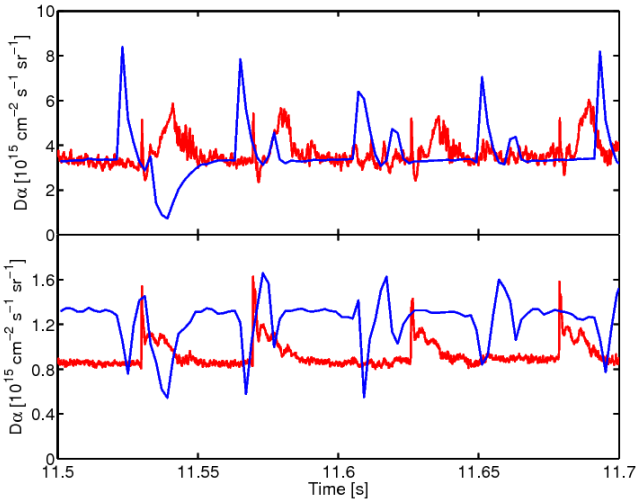

Figure 11. Time evolution of measured D_α emission from visible spectroscopy diagnostics (red colour) vs. modelled D_α from JINTRAC synthetic diagnostics (blue) for the inner (top) and outer (bottom) divertor region for steady-state H-mode conditions at 11 s < t < 12 s at high ELM frequency f_{ELM} ~ 43 Hz with ΔW_{ELM} ~ 90 kJ in #90224.

4. Modelling of the H-mode termination phase

The simulations of the end of the quasi-stationary H-mode phase at 11 s < t < 12 s that have been described in the previous section have been continued for the H-mode termination phase when the auxiliary power is gradually ramped down to determine whether the integrated transport and source model applied in JINTRAC is capable to reasonably reproduce the observed W transport characteristics in this phase as well. Simulations have been performed for the discharge without ELM control (#90223), in which core W accumulation takes place in the H-mode termination phase, and is, therefore, ideal to test the capabilities of our integrate modelling to reproduce accurately the experiment. Apart from the reduction in P_{AUX}, the H-mode termination phase only differs from the quasi-stationary H-mode phase from the modelling point of view in terms of the applied ELM frequency which has been set to half of the frequency in quasi-stationary H-mode. Compared to the experiment in which the ELM frequency is strongly fluctuating for t > 12 s, this may be a simplified but still reasonable estimate, as the time-averaged ELM frequency in that phase indeed corresponds roughly to ~50% of the natural ELM frequency in the quasi-stationary H-mode. The reduction in f_{ELM} may be caused by a reduction in heat flux from the core due to lower P_{AUX} and increased $P_{rad,core}$ and an increase in anomalous transport in the pedestal as P_{net} approaches P_{L-H}, which leads to an increase in the required time for the re-establishment of the pedestal after an ELM crash and for the increase in normalised pedestal gradient to the MHD limit. According to estimates of the time evolution of the energy content from equilibrium reconstruction calculations, the energy loss per ELM remains roughly unchanged in the H-mode termination phase. In the simulation, ΔW_{ELM} has therefore been kept constant at 140 kJ.

A selection of time traces for the complete simulation of the late quasi-stationary H-mode and the H-mode termination phases for the case without ELM control (#90223) are displayed in Fig. 12. As can be seen in that figure, the temperature in the very core of the plasma that has already started to decrease in the late quasi-stationary H-mode phase is much further reduced in the H-mode termination phase with the temperature profile becoming hollow. This fast reduction in core temperature can be explained by self-accelerating W core accumulation and an associated pronounced rise in core radiation. The latter is enhanced even further as the temperature is reduced and the W cooling rates increase at lower temperature (for T_e in the keV range). The barycentre location of the core radiation profile is shifted from the edge to the very core, i.e. the W radiation near the magnetic axis becomes more important than the W radiation in the edge region due to the peak in W density in the ETB zone.

Due to the reduction in f_{ELM} in the H-mode termination phase, $<D/\chi>_t$ in the ETB is reduced leading to an increase in n_{ped}/T_{ped} and a concomitant further degradation of the neoclassical temperature screening efficiency in the barrier region. As the anomalous transport within the ETB is predicted to increase with P_{net} slowly approaching P_{L-H}, the pressure on top of the pedestal is gradually reduced. In the core region, $|\nabla T|$ is reduced due to the strong increase in core radiation, while $|\nabla n|$ is increased due to a reduction in n_{ped} and an increase in n_{ax}, the latter being partly triggered by a widening of the central zone with zero anomalous transport caused by the reduction of the inverse normalised temperature gradient length L_T^{-1} below the stiffness threshold (cf. Fig. 14). Similar to the change in neoclassical W transport conditions in the edge region, the neoclassical W screening efficiency also deteriorates in the core due to the reduction in $|\nabla T|/|\nabla n|$.

The effect of the degradation in core and edge W transport conditions and the reduction in ELM frequency is visualised in Fig. 13. At the beginning of the H-mode termination phase, the peak in W density in the barrier region is widened which is a consequence of the deterioration in neoclassical W transport conditions in the barrier and an enhanced convective influx of W from the SOL. Later on, the width and height of the W density peak in the edge

start to shrink as the pedestal pressure is reduced and thus the neoclassical W transport decreases in absolute terms. The ELM-induced transport of W particles from the edge to the core appears to be slightly increased due to less favourable neoclassical W transport in the core. For the same reason, the W density in the very core is further increased until it even exceeds the peak density of W in the edge. At a core W density level of $n_{W,ax} \sim 3 \cdot 10^{17}/m^3$, a radiative collapse occurs in the very core of the plasma with the temperature dropping down to a few hundred eV.

Sawteeth may help to slightly alleviate or delay the process of W accumulation in the core at least in the early H-mode termination phase. The sawtooth frequency increases at first as the core temperature is reduced and the core resistivity is increased, however, in the later H-mode termination phase, the sawteeth disappear due to a redistribution of current density taking place in the very core. As the temperature profile becomes hollow, the current density also develops an off-axis peak that is associated with the shape of the temperature profile. As a consequence, the safety factor is increased in the very core and it remains above unity preventing sawtooth activity in this phase. In conclusion, sawteeth help to mitigate core W accumulation but their effect is predicted to be comparably small in the examined H-mode termination case. Sawteeth are expected to be present only in phases of the H-mode termination with non-severe core W accumulation, i.e. at times when the core temperature profile remains peaked.

Comparing modelled vs. measured time traces for the plasma core energy and radiation and the axial electron temperature (cf. Fig. 15), reasonable agreement is achieved for the stationary H-mode and the early H-mode termination phases ($t < 12.25$ s), however, the evolution towards a radiative collapse in the later H-mode termination phase appears to be exaggerated in the simulation with the core energy and $T_{e,ax}$ dropping much faster as compared to the experiment. This is due to some extent to the non-consideration in the simulation of the delay between injected and deposited NBI power due to NBI particle thermalisation so that the effective decrease of NBI power in the experiment occurs with some delay with respect to that in the modelling (typically the NBI ion slowing down time in these plasma conditions is ~50 ms). In addition, the discrepancy in modelled vs. measured energy decay times could also be associated with the appearance of intermittent L-mode phases after ELM events in the experiment when P_{net} is suddenly reduced due to the heat flux from the core being consumed for the re-establishment of the pedestal. Such intermittent phases do not occur in the simulation; this is due to the slight smoothing of the term dW_{th}/dt with a characteristic smoothing time of one millisecond in the evaluation of P_{net} for comparison with $P_{L\text{-}H}$, which is required in the modelling to provide numerical stability for simulations near the L-H transition. In principle, intermittent L-mode periods are beneficial for the reduction or deceleration of core W accumulation, as anomalous transport is considerably increased in these periods in the entire plasma region causing a redistribution of W from the very core to exterior regions leading to net W expulsion from the core. At $t > 12.5$ s, the plasma enters a dithering phase in which the plasma changes between intermittent L-mode and H-mode phases at high frequency in the experiment. Although this phase has not been modelled, there are indications that the dithering has helped in the experiment to avoid a complete radiative collapse and to allow for a recovery of the temperature in the core before the plasma enters stationary L-mode conditions. A detailed investigation of the L-H dithering and H-L transition phases will be the subject of future modelling studies.

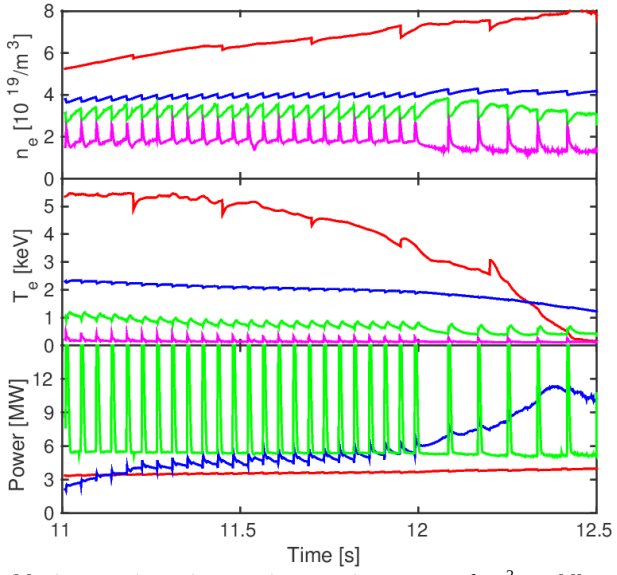

Figure 12. Top: $n_{e,ax}$ (red), $\langle n_e \rangle$ (blue), $n_{e,ped}$ (green), $n_{e,sep}$ (magenta), in units of m^{-3}, middle: $T_{e,ax}$ (red), $\langle T_e \rangle$ (blue), $T_{e,ped}$ (green), $T_{e,sep}$ (magenta) in eV, bottom: P_{L-H} (red), $P_{rad,core}$ (blue), P_{net} (green) in W, for JINTRAC simulation of steady-state H-mode and H-mode termination phases at 11 s < t < 12.5 s at low natural ELM frequency f_{ELM} < 24 Hz with ΔW_{ELM} ~ 140 kJ in #90223.

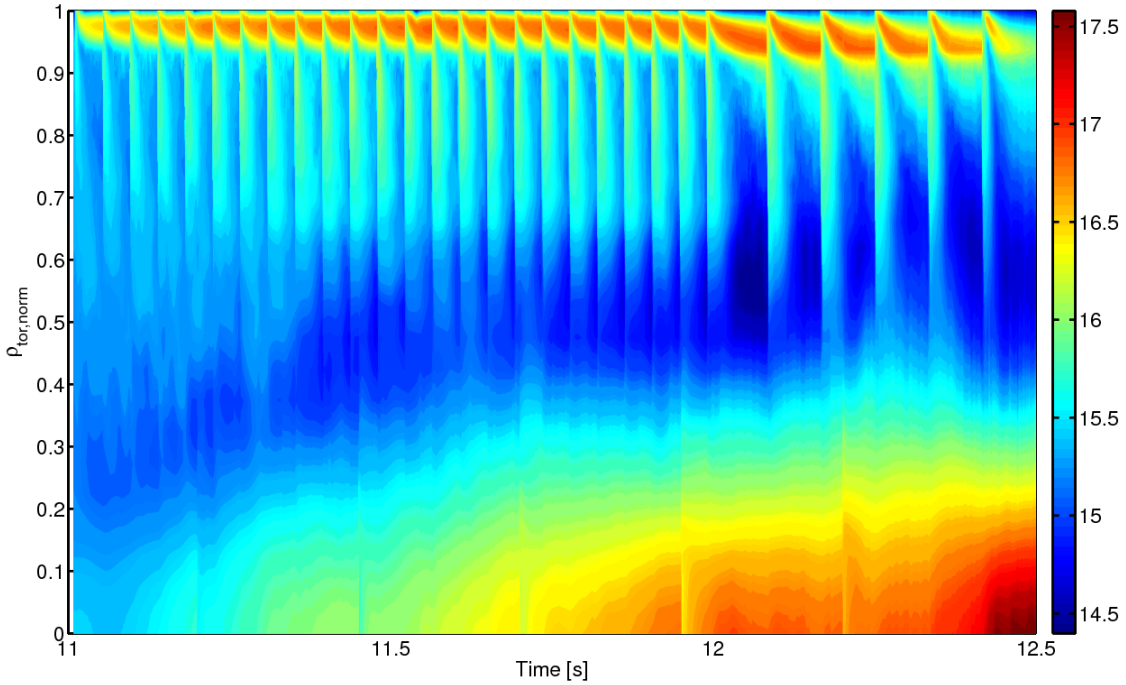

Figure 13. Log-10 contour plot of the W density in m^{-3} in the core and edge regions 0.0 < ρ_{norm} < 1.0 for the JINTRAC simulation of steady-state H-mode and H-mode termination phases at 11 s < t < 12.5 s at low natural ELM frequency f_{ELM} < 24 Hz with ΔW_{ELM} ~ 140 kJ in #90223.

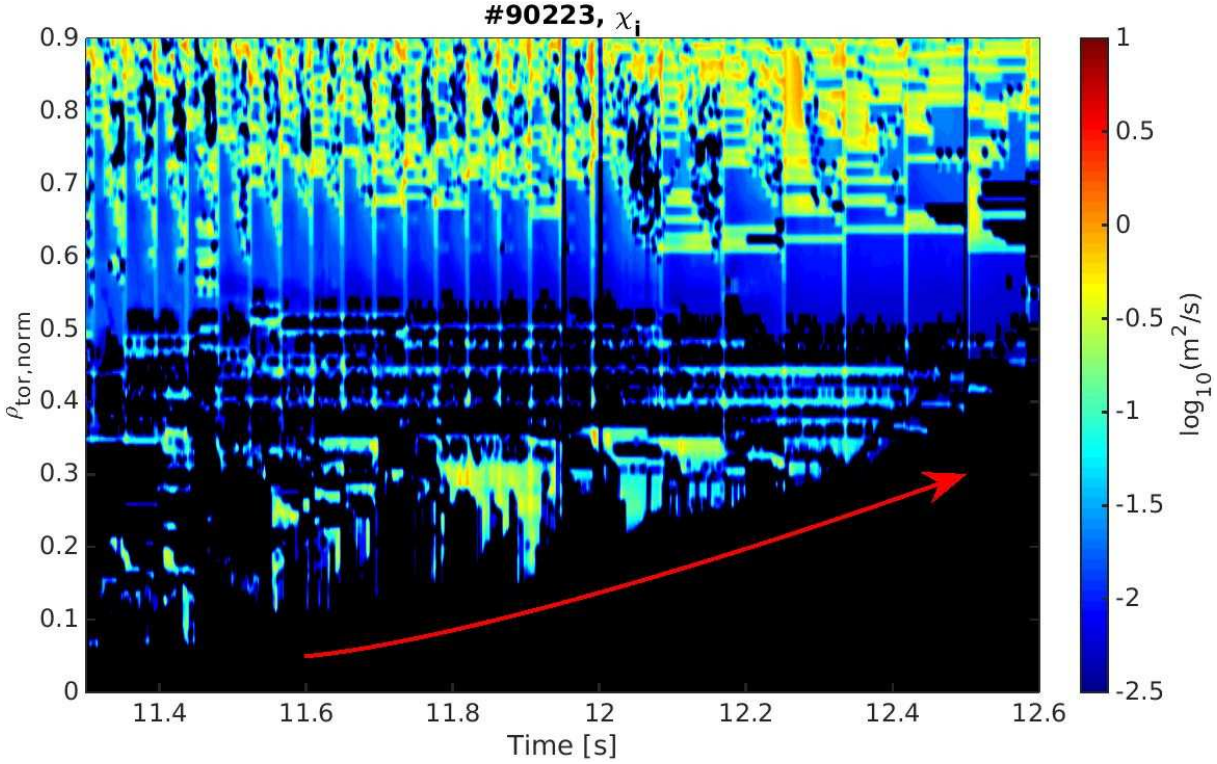

Figure 14. Log-0 contour plot of the anomalous ion heat conductivity in the core region 0.0 < ρ_{norm} < 0.9 for the JINTRAC simulation of steady-state H-mode conditions at 11 s < t < 12.5 s at low natural ELM frequency f_{ELM} < 24 Hz with ΔW_{ELM} ~ 140 kJ in #90223. The red arrow indicates the expansion of the central region without anomalous transport with time.

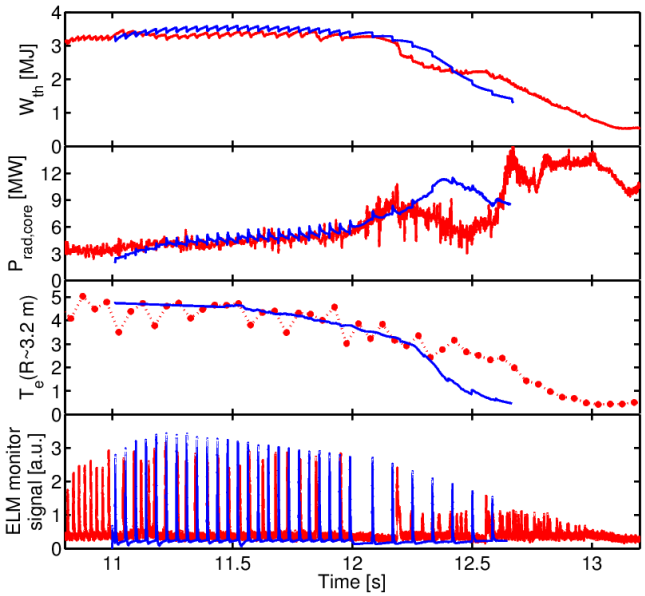

Figure 15. Top: Measured core energy (red colour, from MHD equilibrium analysis) vs. JINTRAC modelled core energy evolution (blue colour) in MJ, top-middle: total core radiation from bolometer measurement (red colour) vs. JINTRAC modelled core radiation (blue colour) in MW, bottom-middle: measured (red, from HRTS) vs. JINTRAC modelled electron temperature near magnetic axis in keV evaluated at $R_{mid,out}$ ~ 3.1 m near the magnetic axis, bottom: ELM monitor signal derived from Be emission measurement (blue) and simulated SOL radiation (red), for steady-state H-mode and H-mode termination phases at 11 s < t < 12.5 s at low natural ELM frequency f_{ELM} < 24 Hz with ΔW_{ELM} ~ 140 kJ in #90223.

Complementary to the abovementioned comparison between modelling and measurement results for the H-mode termination phase, attempts were also made to assess how well the local W core concentration and details related to the spatial re-distribution of W in the plasma core region are reproduced in the simulations. To this end, the line-averaged core radiation

power density measured by bolometer diagnostics for the LFS region, where W tends to accumulate due to plasma rotation so that the total emissivity may be dominated by W-induced radiation, has been compared with modelled bolometer signals from synthetic diagnostics implemented in JINTRAC. In the calculation of the synthetic diagnostic signals, the rotation-induced poloidally asymmetric distribution of W that leads to a poloidally asymmetric radiation pattern has been taken into account by direct application of a factor $\exp(M^*(\rho,\theta)/2)/\langle\exp(M^*(\rho,\theta)/2)\rangle$ to the radiation power density (assuming that the density dependence of the W cooling rate is negligible). Here the Mach number is given by $M^*(\rho,\theta) = m^*\Omega(\rho)^2R(\rho,\theta)^2/T_i(\rho)$ for ions with the effective impurity mass m^*, as described in [Koskela PPCF 2015]. Contour plots of the modelled core radiation power density including this factor are shown in Fig. 16 for three selected times between ELMs to illustrate the variation in the radiation pattern between the early stationary H-mode and the later H-mode termination phases. While the radiation is significant in the plasma pedestal region due to the presence of a peak in W density, it is much smaller (an order of magnitude lower) in the outer core region, whereas it is largest and strongly increases with time near the magnetic axis. Due to the low toroidal rotation in the edge region and significant rotation in the core, the radiation in the pedestal appears to be uniformly distributed in the poloidal direction, while the radiation in the core is poloidally asymmetric. This asymmetry is enhanced with time in the H-mode termination phase due to the ion temperature dependence of M^* with the ion temperature in the centre decreasing with time, as W radiation increases.

A comparison of measured vs. calculated integrated LFS radiation is shown in Fig. 17 for three bolometer lines of sight corresponding to signals $P_{bol\ 02\text{-}04}$ which are indicated in Fig. 16. While signal $P_{bol\ 02}$ provides information about the radiation in the plasma edge region, $P_{bol\ 03}$ and $P_{bol\ 04}$ may be representative for the radiation emitted in the outer and inner core regions respectively. Due to the inclination of the lines of sight towards the LFS, these signals should not be affected by perturbations caused by transient variations in divertor radiated power e.g. due to ELMs. Remarkable agreement in absolute terms is achieved for the edge and inner core radiation between modelling and experiments, though the outer core radiation is overestimated in the simulation. Trends in the time evolution showing a temporary increase in radiation for all bolometer signals in the H-mode termination phase are also reasonably well reproduced. This is a strong indication that the details in the spatial and temporal characteristics of the core W distribution are properly described with the set of integrated transport models that have been applied in the simulations. In particular, the good agreement for the time evolution of the local radiation in the three plasma regions considered confirms that the W density profile shape variation in the core and edge regions is essentially determined by neoclassical effects. The fact that the line of sight crossing the pedestal provides a larger line-averaged radiation signal in the experiment than that further inwards ($P_{bol\ 03} < P_{bol\ 02}$) is consistent with the modelled W density peak in the pedestal region obtained in the simulations; therefore we can conclude that W indeed seems to accumulate strongly in a narrow region near the separatrix in the experiment as predicted in the simulations. Further inwards the W density reaches a minimum in the outer core region where anomalous W transport also plays an important role, while in the inner core the W density can increase again depending on whether screening or accumulation takes place, which depends on plasma conditions. This minimum W value at the outer core may be even lower in the experiment than in the simulations, as $P_{bol\ 03}$ is overestimated in the simulations. This overestimation and the fact that perturbations in $P_{bol\ 03}$ that are associated with ELM events are well visible in the simulation but not in the experiment is an indication that the ELM affected core plasma region for W transport that is indirectly prescribed with the empiric ELM model used in these simulations may be too wide. Furthermore, these differences could

also be partly explained by the possibility that the effect of a partial inwards diffusion of W as a direct consequence of the ELMs as described in the previous section may actually be much more benign in the experiment than predicted in the simulations.

The fact that the experimental time evolution in radiation from the inner core region is fairly well followed in the simulation, including a slight increase in radiation that has been predicted to occur already in the stationary H-mode phase at natural ELM frequency, is a good indication that the rotation-induced enhancement in neoclassical transport is reasonably well described with the model proposed in [Romanelli PPCF 1998], as the absolute level of W density in the core is strongly dependent on predictions based on this model. It should be noted though that the accumulation of W in the innermost core region near the magnetic axis that is not well covered by signal $P_{bol\,04}$ may be overestimated in the simulations.

The overall level of agreement in measured vs. modelled P_{bol} signals that has been achieved also confirms that assumptions for the W cooling rate taken from [Pütterich PPCF 2008] are reasonably adequate. Known uncertainties for these cooling rates seem to point to the possibility to even better reproduce measured core radiation patterns by consideration of improved cooling rate estimates that are known deviate from previous calculations especially in a temperature range $T_e < \sim 1$ keV. Although work for the determination of such estimates is ongoing (cf. e.g. [Solano EPS 2016, Henderson PPCF 2017]) some preliminary results have been used to reassess the radiation obtained. Without rerunning the simulations, the core radiation has been recalculated with the modelled temperature and density conditions applying the new results for the W cooling factor, and the synthetic diagnostic bolometer signals have been re-processed. As the deviation in the new W cooling rates is small with respect to [Pütterich PPCF 2008] at temperatures $T_e > \sim 1$-2 keV, significant discrepancies are expected to be present mostly in the pedestal region where temperatures are much lower. Fig. 17 includes a time trace for the reprocessed $P_{bol\,02}$ signal showing that this is indeed the case. An improvement in the agreement of the modelled $P_{bol\,02}$ with that from the measurement is achieved in absolute terms. In addition to this, it is worth noting that the modelled dynamic evolution of $P_{bol\,02}$ during ELM cycles seems to approach the experimental one only with the reassessed W cooling rates, with the strong positive excursions occurring during or immediately after ELMs for the previous W cooling rates being reduced or even reversed. This is a consequence of a much lower temperature dependence of the new W cooling rates at $T_e > 1$ keV. While the radiation is temporarily increased in the old estimates when the outer pedestal zone is heated up during and after the arrival of the ELM induced heat pulse, as the W radiation efficiency was predicted to increase with temperature, this effect is significantly reduced with the new estimates.

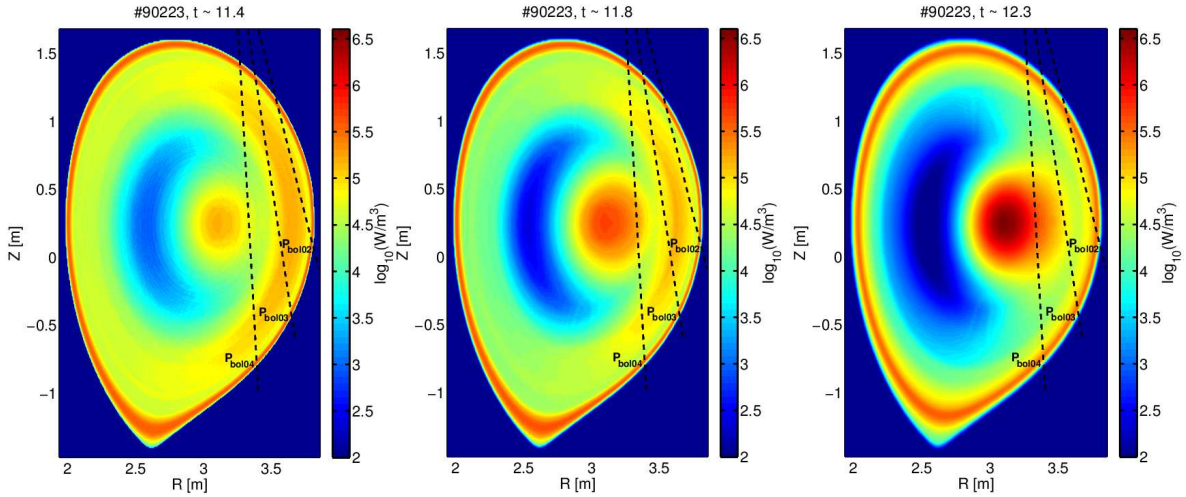

Figure 16. Contour plots of modelled inter-ELM core radiation power density considering a rotation-driven poloidally asymmetric W density distribution for the steady-state H-mode and H-mode termination phases at t ~ 11.4 s (left), ~ 11.8 s (middle), and ~12.3 s (right) for the simulation at low natural ELM frequency f_{ELM} < 24 Hz with ΔW_{ELM} ~ 140 kJ in #90223. Bolometer lines of sights for the measurement of locally emitted radiation in the LFS region as shown in Fig. 17 are indicated by black dashed lines in the left contour plot.

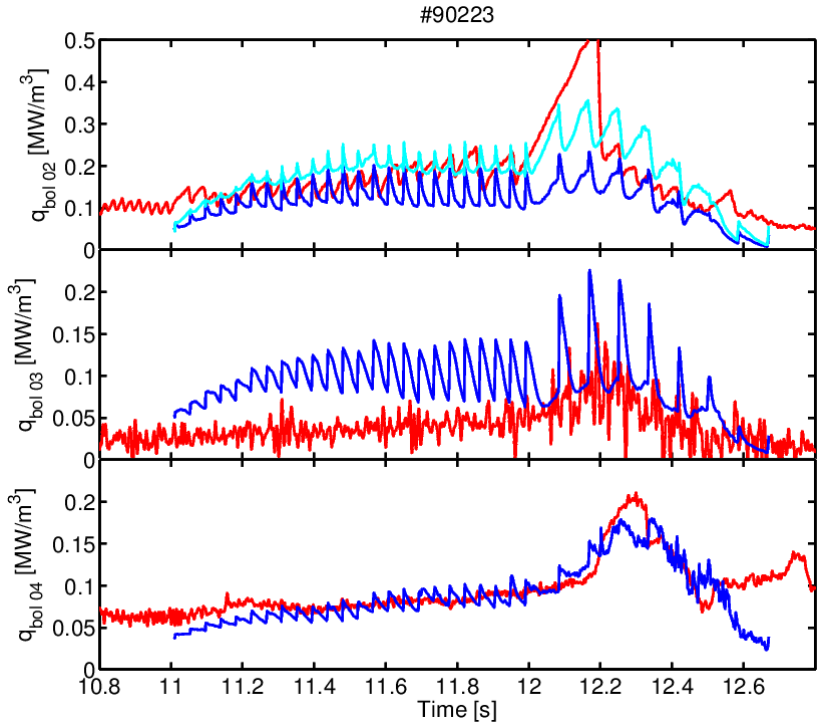

Figure 17. Top: Line-averaged LFS radiation power density as measured by bolometer diagnostics (red colour) vs. JINTRAC modelled integrated power density from synthetic diagnostics calculations considering a rotation-driven poloidally asymmetric W density distribution (blue colour), for the steady-state H-mode and H-mode termination phases at 11 s < t < 12.65 s at low natural ELM frequency f_{ELM} < 24 Hz with ΔW_{ELM} ~ 140 kJ in #90223. Top: Integrated power density emitted in the edge, middle: in the outer core, bottom: in the inner core LFS region. The corresponding bolometer lines of sight are indicated in Fig. 16. The bolometer signal covering the radiation losses in the edge LFS region being re-evaluated with improved W cooling rate estimates for low temperatures < ~1 keV is shown in cyan colour.

5. Core W transport dependencies on core sources and transport conditions

To study the detailed effects of ELM control and core plasma energy/momentum/particle sources on core W accumulation during the H-mode termination phase, dedicated simulations with JINTRAC core+edge have been performed. These simulations use the results of the full JINTRAC core+edge+SOL for the edge and SOL plasma (see Sections 3 and 4) as boundary conditions and concentrate on the dependency of the W transport in the confined plasma on physics processes in the H-mode termination phase. In principle, these studies could also be done with the full JINTRAC core+edge+SOL model used in Section 3 and 4 but the CPU required is very large and it is, therefore, not practical to perform studies were a wide range of dependencies are explored.

5.1. Effect of ELM control on W transport in H-mode termination

Simulations have been carried out for the H-mode termination phase in discharges with and without continued ELM control by kick application (#90224 vs. #90223) considering only core and edge transport. In these runs, transport due to ELMs is described by the continuous ELM model [Parail NF 2009], and boundary conditions are imposed at the separatrix, with the influx of Be and W impurities being feedback controlled against the experimental Z_{eff} and P_{rad}, respectively. Other simulation conditions are identical with those applied in the core+edge+SOL simulations described in the previous sections. Further details in simulation conditions are given in Section 2. The modelling results confirm that the reduction in ELM frequency without ELM control induces a reduced time-averaged edge particle vs. heat transport due to the lower D/χ ratio in the ETB in the phases between ELMs and possibly less diffusion by the natural ELMs. This gives rise to the formation of increased density gradients in the ETB and less efficient temperature screening for W. As a consequence, a larger amount of W is transported to the plasma core, leading to W accumulation and increased radiation near the magnetic axis, leading to the appearance of hollow temperature profiles and a radiative collapse associated with an early H-L transition due to strongly enhanced core radiation.

A comparison between measured and modelled time traces describing relevant core plasma properties for #90224 (controlled ELM termination) vs. #90223 (uncontrolled ELM termination) is shown in Figs. 18-21. The differences regarding ELM control for these discharges is accounted for in the JINTRAC core+edge simulations presented here through a difference in the applied W influx at the separatrix (accounting for a difference in the W sputtering source) and reduced time-averaged (ELM induced) particle diffusivity in the ETB in the phase without ELM control in #90223. Otherwise, the two discharges are identical both in terms of experimental and modelling conditions. Although the time for the appearance of hollow temperature profiles and for the H-L transition cannot be exactly matched and the core W concentration seems to be reduced more quickly in the experiment in the L-mode phase for #90223 than in the modelling, the main core plasma properties can be reasonably well reproduced for the H-mode termination phase in the simulations for these two discharges. These results strengthen the hypothesis that the likelihood of core W accumulation increases for reduced ELM frequencies due to reduced neoclassical screening in the pedestal, as already pointed out in Section 3. In addition, the reasonable agreement with experiment confirms the general validity of the core transport model assumptions applied for the prediction of the plasma evolution in the H-mode termination phase in the previous section.

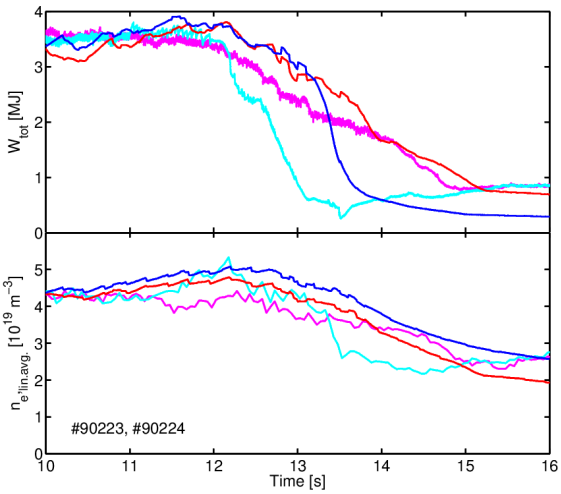

Figure 18. Comparison of measured (magenta/cyan) vs. simulated (red/blue) time traces for the H-mode termination phase in #90224 with ELM control in the termination phase (magenta/red) and #90223 no ELM control in the termination phase (cyan/blue). From top to bottom: total energy content and line-averaged electron density.

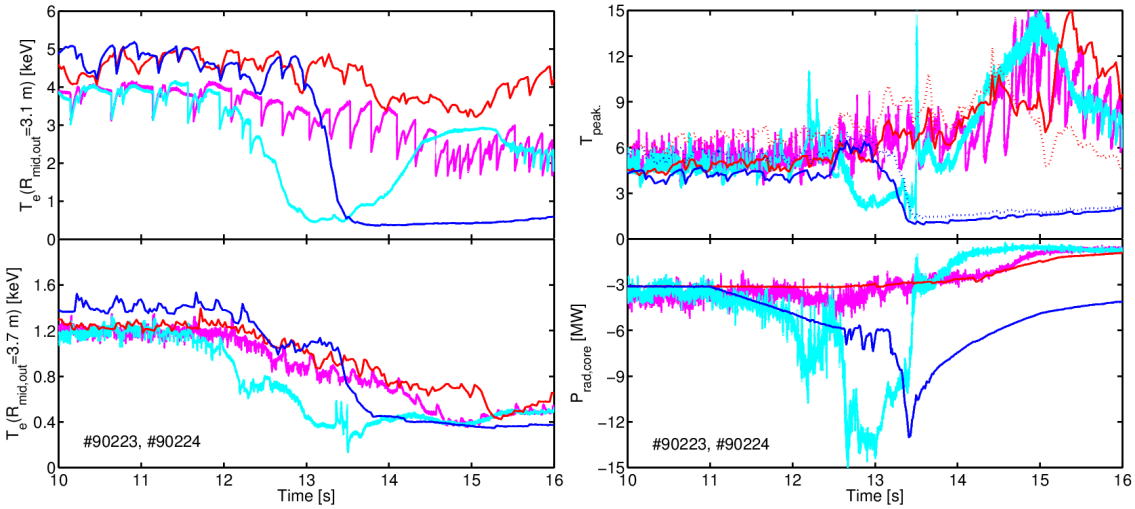

Figure 19. Comparison of measured vs. simulated time traces for the H-mode termination phase in #90224 and #90223, same colour code as for Fig. 18. Left: core electron temperature (top, evaluated at $R_{mid,out}$ = 3.1 m) and edge electron temperature (bottom, evaluated at $R_{mid,out}$ = 3.7 m), right: peaking factor for electron (solid) and ion temperature (dotted), evaluated as $T(R_{mid,out} = 3.1\ m)/T(R_{mid,out} = 3.75\ m)$ (top) and core radiation (bottom).

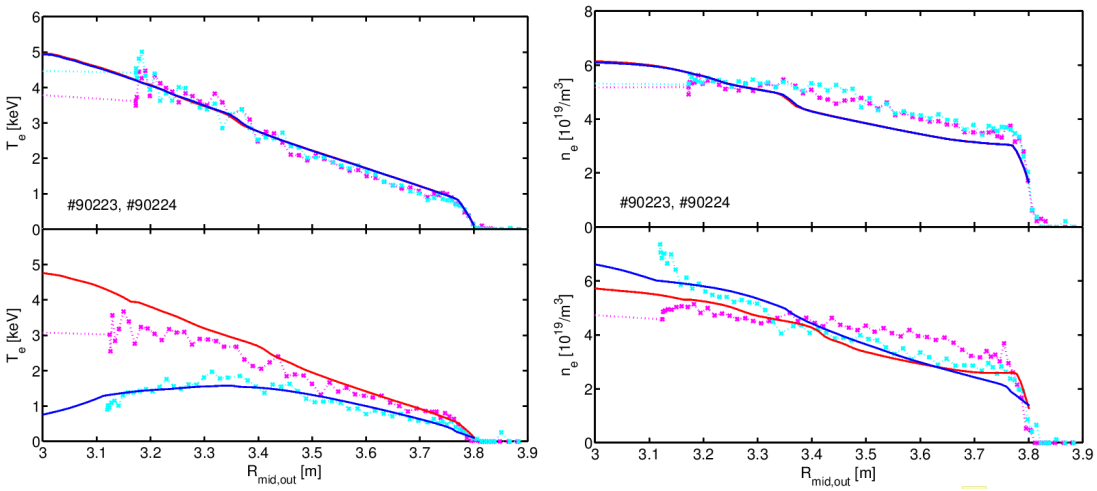

Figure 20. Comparison of measured vs. simulated T_e and n_e profiles (from left to right) at t = 10 s (top) and t = 12.75 s (bottom) in #90224 and #90223, considering a time shift of ~0.75 s for the modelled data to match experimental H-L transition times, same colour code as for Fig. 18.

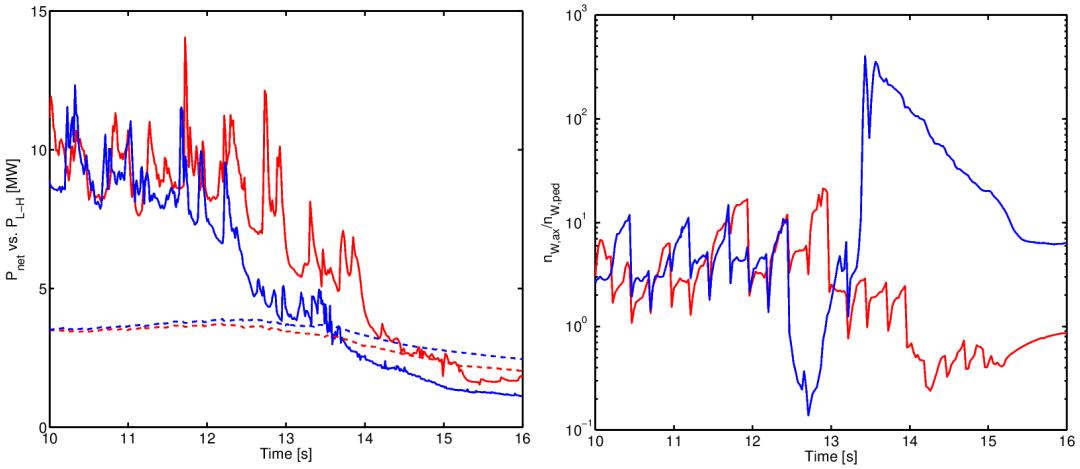

Figure 21. Simulated time traces for the H-mode termination phase in #90224 (red) and #90223 (blue). Left: P_{net} (solid) vs. P_{L-H} (dashed), right: W density peaking factor $n_{W,ax}/n_{W,ped}$.

5.2. Effect of NBI momentum and particle sources on W transport in H-mode termination

As mentioned in Section 1, a long H-mode termination phase is advantageous for ITER high Q plasma scenarios as it facilitates plasma position control in this phase and also minimizes power fluxes to the plasma facing components. The JET experiments emulated this ITER-like plasma behaviour by ramping down slowly the additional heating power, which is dominated by NBI in these experiments. However, other differences remain regarding the termination of H-modes in JET and ITER which are associated with the larger (normalized to ITER) core particle sources and torque provided by the (positive ~100 keV energy) NBI in JET compared to the negative NBI (~ 1 MeV) in ITER. Both these factors are known to affect W transport by modifying the plasma density as well as the toroidal rotation profile in the plasma centre in JET in a very different way to that expected in ITER were both NBI-driven core fuelling and plasma toroidal rotation are expected to be small. Dedicated modelling studies have been therefore been performed in order to assess the role of these effects on the W transport and accumulation of these JET H-mode plasmas in the H-mode termination phase.

5.2.1. Effect of NBI momentum sources on W transport in H-mode termination

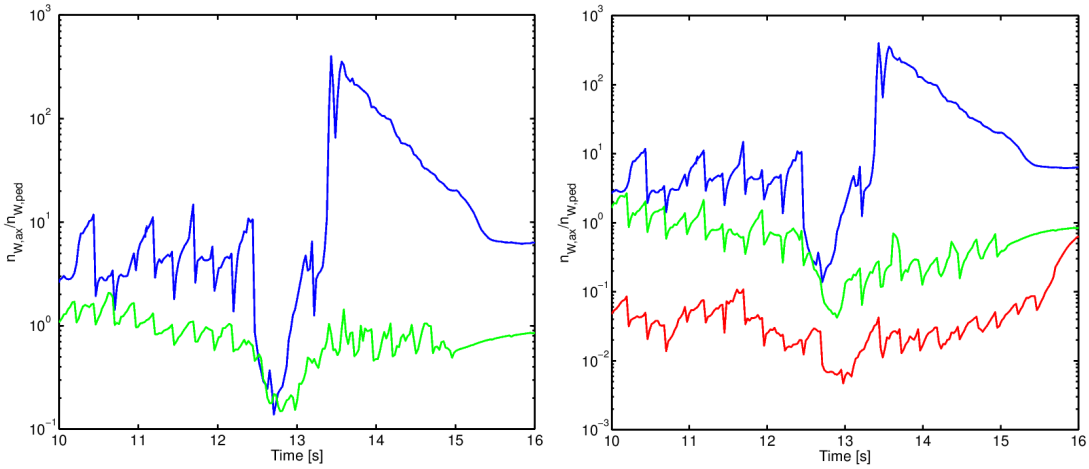

Figure 22. Simulated time traces for the H-mode termination phase in #90223 for the W density peaking factor $n_{W,ax}/n_{W,ped}$. Left: comparison of results obtained with (blue) and without (green) consideration of rotation driven poloidal asymmetry in W distribution affecting neoclassical W transport, right: comparison of results with anomalous core W transport evaluated with GLF23 D_W and v_W (blue), with 50% reduction of D_W and v_W (green) and assuming that W transport is purely neoclassical (red).

As described in [Casson PPCF 2015], neoclassical transport enhanced by poloidal asymmetries can be a crucial mechanism responsible for tungsten accumulation in the central core region of plasmas at high rotation. For the H-mode termination in #90223 (no ELM control), this is confirmed by a test simulation in which the neoclassical W transport has been calculated assuming that there is no rotation driven poloidal asymmetry in W distribution (i.e. neglecting the correction terms from [Romanelli PPCF 1998]). As shown in Fig. 22 (left), W core accumulation can be avoided in that case. We can thus conclude that in the H-mode termination phase of these JET H-modes the toroidal rotation produced by NBI indeed plays an essential role in the occurrence of W accumulation by providing enhanced unfavourable inwards directed W neoclassical transport in the central plasma region where maximum rotation values are achieved. For the outer plasma region which have a favourable outwards directed W convective neoclassical transport due to temperature screening this effect is only marginal, as rotation is low in the periphery.

In addition to neoclassical W transport, the net time-averaged anomalous W transport in the plasma core also seems to be important to produce core W accumulation in the H-mode termination phase in these experiments. Fig. 22 (right), shows simulations with the baseline GLF23 W anomalous transport coefficients (D_W and v_W) and with various levels of reduction of such coefficients, producing very different results regarding W accumulation in the H-mode termination phase. When D_W and v_W are reduced by more than 50%, W does not accumulate near the magnetic axis in #90223 (without ELM control) despite the inclusion of the toroidal rotation driven neoclassical transport enhancement in the simulations.

5.2.2. Effect of NBI particle sources on W transport in H-mode termination

In addition to the momentum source, the particle source associated with NBI heating is also expected to affect core W transport as it increases the main ion density gradient in the plasma core, which leads to a more inwards directed neoclassical convective W velocity. The importance of this effect has been assessed for the H-mode termination phase in #90223 (without ELM control) by comparing JINTRAC core+edge transport simulations with the NBI heating and particle source and artificially removing the particle source while considering the heating source. The results are illustrated in Fig. 23; in line with previous findings for the stationary phases of hybrid scenarios [Mantica EPS 2014], it is found that the NBI particle source is an important factor determining the accumulation of W both in the stationary H-mode phase of JET ILW discharges as well as in the H-mode termination phase.

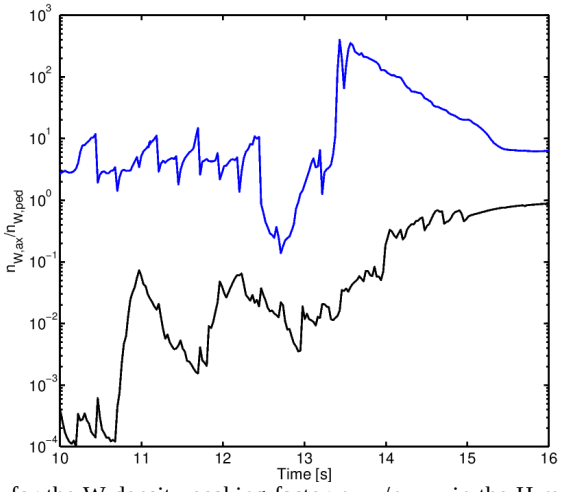

Figure 23. Simulated time traces for the W density peaking factor $n_{W,ax}/n_{W,ped}$ in the H-mode termination phase in #90223. Comparison of results with (blue) and without (black) NBI particle source.

5.3. Effect of ICRH on W transport in H-mode termination

Experiments in the stationary phases of JET ILW H-modes clearly indicate that core W accumulation is significantly reduced by including ICRH in the auxiliary heating mix. This is especially clear in the late H-mode termination phase where a pronounced increase in core temperature gradients can be observed, which contributed to outwards neoclassical convection of W and W accumulation avoidance [de la Luna 2017]. However, in the experiments reported here it was not possible to prevent W accumulation by applying ICRH heating when ELMs were not actively controlled, although the applied level of ICRH power was ~1-2 MW due to limitations in coupling efficiency in the ELMy H-mode plasma edge conditions.

To assess the potential effects of higher levels of ICRH heating on W transport in the H-mode termination phase, simulations for this phase in discharge #90223 have been repeated with various levels of ICRH power and the results are presented in Fig. 24. These simulations confirm that neoclassical core W transport properties can be affected by ICRH heating but that the effects are only sizeable for higher power levels (P_{ICRH} ~ 4 MW) than those used in the experiments modelled here. The positive effects on W transport (lack of accumulation) are due to a reduction in core ion density vs. ion temperature gradients that increases the outwards directed W neoclassical convection in the plasma core, as described in [Casson PPCF 2015, Mantica EPS 2014]. These modelling results suggest that there is a trade-off between central ICRH power and the required level of ELM control to avoid W accumulation in the termination phase of JET H-modes; the higher the level of ICRH power the less stringent the requirements for ELM control in this phase. Here the differences between NBI (providing heating but also particle and momentum source in the plasma centre) and ICRH (providing only heating) are key for their different effects on W transport.

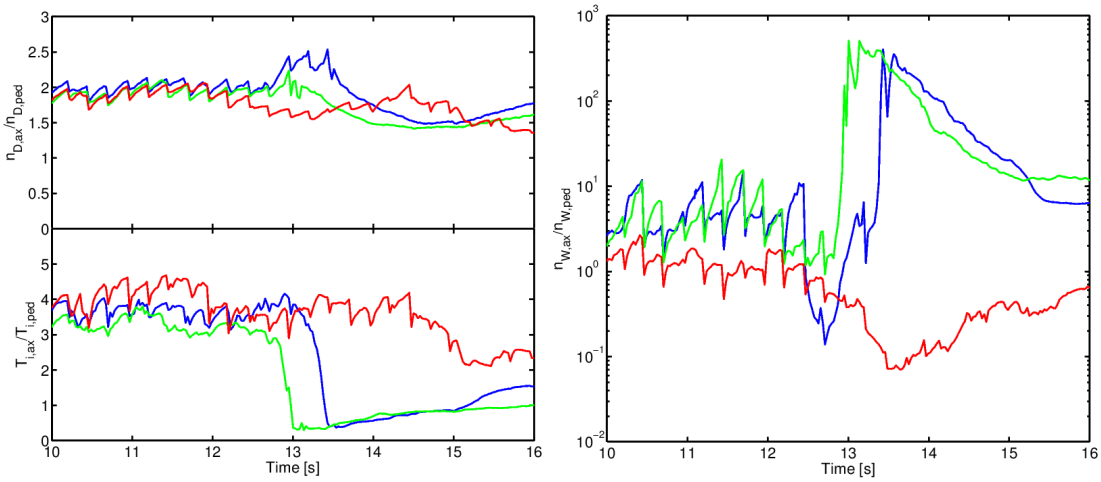

Figure 24. Simulated time traces for the H-mode termination phase in #90223 (without ELM control). Scan in applied P_{ICRH}: ~1 MW (green), ~1.9 MW (blue, experimental value), ~4 MW (red). Left: peaking factors $n_{D,ax}/n_{D,ped}$ and $T_{i,ax}/T_{i,ped}$. Right: W density peaking factor $n_{W,ax}/n_{W,ped}$.

6. Implications for W transport in the H-mode termination phase of the ITER Q=10 baseline scenario

As for JET, core W accumulation may also occur in the H-mode termination phase in the ITER 15 MA/5.3 T Q=10 baseline scenario [Loarte FEC 2016]. Simulations for ITER Q=10 H-mode termination show that decreasing pellet fuelling together with external auxiliary heating is optimum to ensure a slow decrease of the plasma energy and of the alpha heating which facilitates radial position control and minimizes power fluxes to the divertor in this

phase [Loarte NF 2014, Militello-Asp FEC 2016]. However, this leads to the formation of relatively peaked density profiles which can be unfavourable for W transport in the termination phase [Loarte EPS 2015]. To evaluate the effects of the various possible operational strategies to terminate Q=10 H-mode plasmas, the integrated models (JINTRAC core+edge) which have been validated against the JET experiments, as discussed in [Koechl NF 2017] and Sections 3-5 of this paper, have been applied to simulate the H-mode termination phase in ITER Q =10 plasmas.

It should be noted here that in the case of the ITER H-mode operation ELM control is mandatory at this level of plasma current [Loarte NF 2014] so that any simulation for ITER of H-mode termination must assume that ELMs are controlled also during this phase. In addition to the mandatory ELM control, the details on how the heating and fuelling are ramped down in ITER are expected to have a large effect on W transport and accumulation in this phase, as demonstrated in the JET experiments. Therefore studies on the optimisation of the ramp-down of the heating and fuelling schemes to reduce the core W peaking factor $n_{W,ax}/n_{W,ped}$ have been carried out by means of JINTRAC core transport simulations [Loarte FEC 2016] confirming that to a large degree the findings in JET experiments and of the modelling studies in Section 3-5 are also applicable to ITER Q=10 terminations. An example of these ITER modelling studies are shown in Fig. 26 where two cases for the transition from stationary H-mode to L-mode in the ITER 15 MA/5.3 T DT Q~10 baseline scenario are shown. In one of the cases, DT fuelling by pellet injection is immediately removed at the beginning of the ramp-down of the auxiliary power while in the other case pellet fuelling is gradually removed. In both cases gas fuelling is maintained at a constant level as required to maintain the separatrix density at the levels required to ensure radiative divertor conditions in the H-mode transition phase. In the case of a gradual reduction of pellet fuelling, it is possible to reduce the core W peaking factor by an order of magnitude with respect to the case of the sudden pellet fuelling switch-off. This is the result of the improved neoclassical temperature screening of W in the core region by avoiding the formation of large $|\nabla n_i|$ in the plasma core; maintaining some pellet fuelling ensures that the pedestal and the core density decrease with a similar rate thus avoiding large $|\nabla n_i|$ in the core plasma when pellet fuelling is suddenly removed (in such case n_{ped} decreases much faster than n_{core} due to the low fuelling efficiency of neutral gas fuelling in ITER thus leading to large $|\nabla n_i|$ to appear in the core plasma during the H-mode termination phase). This is not the only possible Q =10 H-mode termination operational strategy that allows for a noticeable reduction in core W accumulation in this phase and more detailed studies can be found in [Loarte FEC 2016, Loarte 2017]. Thus we can conclude from these ITER studies with the integrated models validated against JET experiments that it should be possible to avoid W accumulation and to control W transport in the H-mode termination phase of ITER H-modes by appropriate adjustment of the power and fuelling (and ELM control) schemes in this phase.

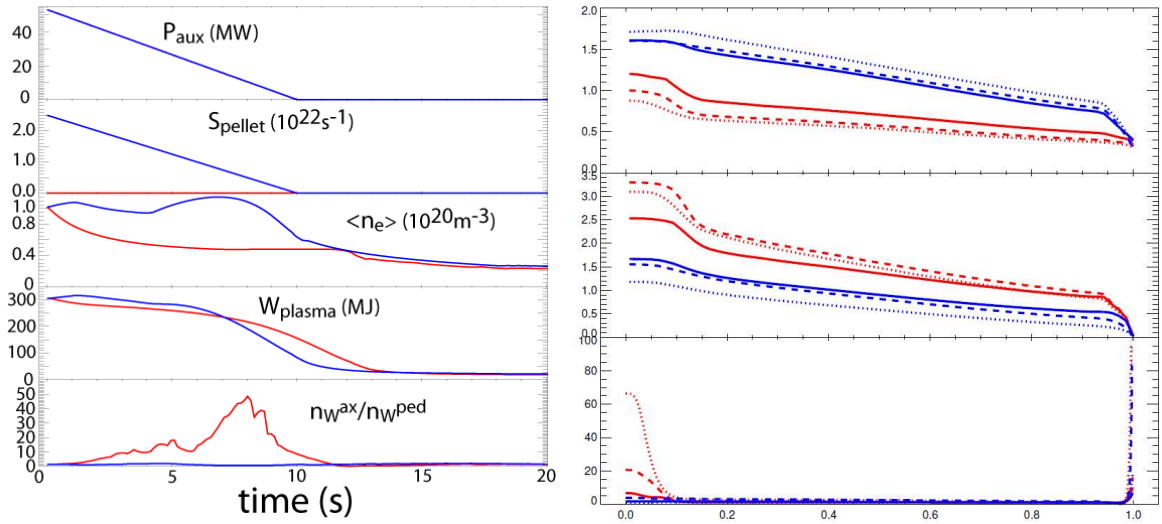

Figure 26. Modelled plasma evolution in the H-mode termination phase of the ITER Q=10 15 MA/5.3 T DT baseline scenario from JINTRAC core+edge transport simulations. Cases with low core W accumulation and gradually reduced core pellet fuelling (blue colour) and with moderate core W accumulation and immediate stop of pellet fuelling at t ~ 0 s (red colour) are compared. Left, from top to bottom: Time traces of auxiliary power, pellet particle fuelling rate, $<n_e>$, core plasma energy, W density peaking factor $n_{W,ax}/n_{W,ped}$. Right, from top to bottom: Core profiles of electron density (in 10^{20} m^{-3}), ion temperature (in keV) and normalised W density $n_W(\rho_{norm})/n_{W,ped}$ for t = 3 s (solid), t = 5 s (dashed) and t = 7 s (dotted).

While the results of the JINTRAC core+edge ITER simulations above are rather optimistic regarding the robustness of the control of W transport in the H-mode termination phase compared to JET, it is important to remark that there are significant differences between ITER and JET and that many uncertainties remain, as summarized below:

- Following the evaluation given in [Chankin PPCF 2014], the fraction of sputtered W particles that are not immediately re-deposited at the target plates after a few gyrations is expected to be well below a percent for the expected ITER target conditions during ELMs, while there are indications that it may be significantly larger during ELMs in JET plasmas as described in Section 3. If W sputtering between ELMs can be considered as negligible, the effective W sputtering yield may then be lower in ITER and thus the source of sputtered W particles in H-mode with ELM control may be less critical in ITER conditions.
- Both experimental evidence and modelling results obtained for ELMy H-mode conditions at JET suggest that ELM control schemes may be crucial for the mitigation of the risk of enhanced core W accumulation. Since ELM control schemes are required to be operational and reliable in ITER for the entire H-mode phase of the main ITER scenarios [Lang NF 2013, Loarte NF 2014b], the enhanced W influx to the core at low natural f_{ELM} in the H-mode termination phase seen at JET will not take place in ITER, where a sufficiently high f_{ELM} (or ELM suppression) will have to maintained throughout the H-mode termination phase.
- Since NBI particle and momentum sources are predicted to be reduced in ITER compared to JET in relative terms, the detrimental effects of these sources on neoclassical W transport in the H-mode termination phase that have been assessed in Section 5 are not expected to play a role in ITER thus leading to a higher temperature screening of W in the termination phase in the ITER plasmas compared to JET.
- As the W cooling rates scale inversely with the electron temperature for T_e > ~ 2 keV, the risk for self-accelerating core W accumulation is modelled to be strongly reduced in ITER for the Q~10 ITER baseline scenario with core temperatures predicted to reach values of up to ~30 keV in the H-mode termination phase, which are likely to

exceed those obtained in stationary H-modes [Loarte FEC 2016]. On the contrary, the core temperature at JET quickly drops to a few keV in the H-mode termination phase where peak values for the W cooling rate are achieved and a runaway process of core W accumulation can easily be triggered, as observed both in the experiment and in the simulations. The radiation due to W in the core plasma may thus remain very low in the ITER H-mode termination phase, i.e. it may not affect the local shape of the core temperature profiles. As a consequence, no formation of self-enhanced inwards convection of W is observed even for significant W concentrations evaluated at the pedestal top as large as $n_{W,ped}/n_{e,ped} \sim 4 \cdot 10^{-5}$ in dedicated modelling studies for the ITER H-mode termination phase [Loarte FEC 2016, Loarte 2017].

- For the ETB region, the neoclassical W screening efficiency is also predicted to be significantly enhanced in the ITER Q~10 baseline scenario with the neoclassical W convection being outwards directed for a large range of expected pedestal conditions, provided that the pedestal pressure is determined by MHD constraints [Dux PPCF 2014]. In these conditions, the ratio $(n_i \nabla T_i)/(T_i \nabla n_i)$ between normalised ion temperature and density gradients is increased due to high $n_{i,sep}$ (reducing $|\nabla n_i|$ and increasing n_i in the pedestal) and $T_{i,ped}$ (increasing $|\nabla T_i|$), and the collisionality in the ETB is strongly reduced compared to typical pedestal conditions in present day experiments. As a consequence, the outward directed temperature screening term of the neoclassical W convection becomes dominant and a hollow W density distribution is predicted for the ETB region. It thus seems likely that a low core W concentration can be maintained in ITER even in case of increased W contamination in the SOL caused by W sputtering thanks to the favourable neoclassical transport conditions within the ETB, provided that any inwards directed W transport due to ELMs as discussed in Section 3 remains insignificant.

7. Conclusions

Dedicated experiments have been performed at JET for the assessment of W transport and possible schemes for the mitigation of W core accumulation in the H-mode termination phase including (amongst others) scans in auxiliary heating schemes and active ELM control methods. It has been demonstrated that the sustainment of ELM control and a sufficient level of ICRH heating in the auxiliary heating mix are essential for the control of the W concentration in the exit phase of H-modes with slow (ITER-like) ramp-down of the NBI power in JET. Initial evaluations for ITER with the JET-validated models indicate that avoidance of W accumulation in the H-mode termination phase of ITER Q=10 plasmas should be readily achieved, provided that ELM control is maintained during this phase; this is a mandatory requirement for ITER H-mode operation also for the stationary H-mode phases.

Modelling of experimental results carried out with JINTRAC has highlighted the importance of certain aspects such as the effect of ELM control on W sputtering, particle transport and edge temperature screening, NBI momentum and particle sources and ICRH-assisted heating for the explanation of observed differences in core W transport properties in the H-mode termination phase. In addition, it has shown that the existing integrated core+edge+SOL transport models can appropriately reproduce the plasma evolution in general and the accumulation of W in particular in stationary ELMy H-modes and in the H-mode termination phase of JET discharges. The model assumptions are thus adequate for the prediction of the W transport behaviour in the H-mode termination phase in ITER. Initial results of this application can be found in [Loarte NF 2014, Loarte FEC 2016] and further studies will be summarized in a paper in preparation [Loarte 2017].

Disclaimer: ITER is the Nuclear Facility INB no. 174. The views and opinions expressed herein do not necessarily reflect those of the ITER Organization. This work has been carried out within the framework of the EUROfusion Consortium and has received funding from the Euratom research and training programme 2014-2018 under grant agreement No 633053 and from the RCUK Energy Programme [grant number EP/P012450/1]. To obtain further information on the data and models underlying this paper please contact PublicationsManager@ccfe.ac.uk. The views and opinions expressed herein do not necessarily reflect those of the European Commission.

References

[Braginski RevPP 1965] Braginski V. I., in Leontovich M. A. (ed), Rev. of Plasma Physics, Consultants Bureau, New York, 1965.
[Casson PPCF 2015] Casson, F. J. et al. Plasma Phys. Control. Fusion 57 (2015) 014031.
[Challis NF 1989] Challis C. D. et al., Nucl. Fusion 29 (1989) 563.
[Chankin PPCF 2014] Chankin, A. V., Coster, D. P. and Dux, R. Plasma Phys. Control. Fusion 56 (2014) 025003.
[de la Luna NF 2016] de la Luna, E. et al. Nucl. Fusion 56 (2016) 026001.
[de la Luna 2017] de la Luna, E. et al., to be submitted to Nucl. Fusion 2017.
[Dux PPCF 2014] Dux R. et al. Plasma Phys. Control. Fusion 56 (2014) 124003.
[Erba JET-R 1996] Erba, M. et al. JET Report JET-R(96)07 (1996).
[Eriksson NF 1993] Eriksson, L. G., Hellsten, T. and Willen, U., Nuclear Fusion 33 (1993) 1037-1048.
[Farina FSciTec 2007] Farina D., Fusion Sci. Techn. 52 (2007) 154.
[Groth JNM 2015] Groth, M. et al. J. Nuc. Mat. 463 (2015) 471.
[Henderson PPCF 2017] Henderson, S. S. et al. Plasma Phys. Control. Fusion 59 (2017) 055010.
[Hirshman NF 1981] S.P. Hirshman and D.J. Sigmar, Nucl. Fusion 21 (1981) 1079.
[Houlberg PoP 1997] Houlberg, W. A. et al. Phys. Plasmas 4 (1997) 3230.
[Kirschner EPS 2017] Kirschner, A. et al., 2017 Proc. 44th EPS Conf. on Plasma Physics (Belfast, UK, 26-30 June 2017) I4.111.
[Koechl NF 2017] Koechl, F. et al. Nucl. Fusion 57 (2017) 086023.
[Koskela PPCF 2015] Koskela, T. et al. Plasma Phys. Control. Fusion 57 (2015) 045001.
[Lang NF 2013] Lang, P. T. et al. Nucl. Fusion 53 (2013) 043004.
[Loarte NF 1998] Loarte, A. et al. Nucl. Fusion 38 (1998) 331.
[Loarte PPCF 2003] Loarte, A., et al, Plasma Phys. Control. Fusion 45 (2003) 1549.
[Loarte NF 2014] Loarte, A. et al. Nucl. Fusion 54 (2014) 123014.
[Loarte NF 2014b] Loarte, A. et al. Nucl. Fusion 54 (2014) 033007.
[Loarte EPS 2015] Loarte, A. et al., 2015 Proc. 42nd EPS Conf. on Plasma Physics (Lisbon, Portugal, 22–26 June 2015) vol 39E, O4.130. http://ocs.ciemat.es/EPS2015PAP/pdf/O4.130.pdf
[Loarte PoP 2015] Loarte, A. et al. Phys. Plasmas 22 (2015) 056117.
[Loarte FEC 2016] Loarte, A. et al. 26th Int. Conf. on Fusion Energy (Kyoto, 2016).
[Loarte 2017] Loarte, A. et al., to be submitted to Nucl. Fusion 2017.
[Militello-Asp EPS 2013] Militello-Asp, E. et al., 2013 Proc. 40th EPS Conf. on Plasma Physics (Espoo, Finland, 1–5 July 2013) vol 37D, P2.158. http://ocs.ciemat.es/EPS2013PAP/pdf/P2.158.pdf
[Martin JoP 2008] Martin, Y. R. et al. Journal of Physics: Conference Series 123 (2008) 012033.
[Maggi NF 2014] Maggi, C. F. et al. Nucl. Fusion 54 (2014) 023007.
[Mantica EPS 2014] Mantica, P. et al. 41st EPS Conf. 2014 p. P1.017.
[Naujoks NF 1996] Naujoks D. et al. Nucl. Fusion 36 (1996) 671.
[Neu PoP 2013] Neu R. et al. Plasma of Physics 20 (2013) 056111.
[Parail NF 2009] Parail, V. et al. Nucl. Fusion 49 (2009) 075030.
[Parail JNM 2015] Parail, V. et al. J. Nuc. Mat. 463 (2015) 611-614.
[Pégourié PPCF 2009] Pégourié B. et al., Plasma Phys. Control. Fusion 51 (2009) 124023.
[Porcelli PPCF 1996] Porcelli, F. et al. Plasma Phys. Control. Fusion 38 (1996) 2163.
[Pütterich PPCF 2008] Pütterich, T. et al. Plasma Phys. Control. Fusion 50 (2008) 085016.
[Romanelli PPCF 1998] Romanelli, M. and Ottaviani, M. Plasma Phys. Control. Fusion 40 (1998) 1767.
[Romanelli PFR 2014] Romanelli, M. et al. Plasma and Fusion Research 9 (2014) 3403023.
[Solano EPS 2016] Solano, E. et al., 2016 Proc. 43rd EPS Conf. on Plasma Physics (Leuven, Belgium, 4–8 July 2017) vol 40A, P2.005.

http://ocs.ciemat.es/EPS2016PAP/pdf/P2.005.pdf
[Summers AIP 2007] Summers, H. P. et al., AIP Conf. Proc. 901 (2007) 239.
[Waltz PoP 1997] Waltz, R. E. et al. Phys. Plasmas 4 (1997) 2482.
[Wiesen PPCF 2011] Wiesen S. et al., Plasma Phys. Control. Fusion 53 (2011) 124039.